Available online at www.sciencedirect.com
SCIENCE DIRECT
ELSEVIER
European Journal of Mechanics B/Fluids 24 (2005) 49–70
EUROPEAN JOURNAL OF MECHANICS B/FLUIDS

An accurate modeling of thin film flows down an incline for inertia dominated regimes

Mustapha Amaouche *, Nadia Mehidi, Nawel Amatousse

Laboratoire de physique théorique, université de Bejaia, route de Targa-Ouzemour, Bejaia, Algeria

Received 16 September 2003; received in revised form 17 March 2004; accepted 3 June 2004

Available online 28 July 2004

Abstract

An accurate modeling of a wavy film flow down an inclined plane is developed using the weighted residual technique which was first proposed by Ruyer-Quil and Manneville [Eur. Phys. J. B 15 (2000) 357]. The model includes third order terms in order to better capture the effects of small Weber and high Reynolds numbers. This is made possible by an appropriate refinement of the velocity profile. To this end, a free parameter α acting on the flexibility of the velocity profile is introduced. It is shown, from linear stability analysis that the model follows quite closely, for a suitable choice of α, the Orr–Sommerfeld equation for all Weber and Kapitza numbers. The improvement is of course more substantial in the inertia dominated regimes. Some prominent qualitative and quantitative characteristics of traveling wave solutions are then derived from a simplified version of the model that is before hand converted into a three dimensional dynamical system.
© 2004 Elsevier SAS. All rights reserved.

Keywords: Film flow; Inclined plane; Stationary waves; Chaotic attractors

1. Introduction

The problem of thin viscous film flowing down an inclined plane is relevant to a broad class of natural phenomena such as gravity currents (rain streaming down the wall, river and lava flows ...) and engineering applications ranging from process equipment for heat and mass transfer to chemical reactors. As it is emphasized by Kliakhandler and Sivashinsky [1], a film flow is one of the most experimentally accessible example of the intrinsically unstable extended system. For these reasons and because it both exhibits a rich dynamical phenomenology and offers a relatively simple basic solution to analyze the bifurcation phenomena encountered in more complex situations, this problem has been the subject of intensive studies dating back to Nusselt's paper [2]. We will see that exactly three independent basic parameters appear in the dimensionless equations of the problem; in addition to the inclination angle θ which accounts for the effects of gravity, one can choose, e.g., the Reynolds number R and the Weber number W which respectively give the relative importance of inertia and surface tension effects compared to viscosity ones. In some range of these parameters, experiments have revealed that film waves often exhibit a large spectrum of wave amplitude, wavelength and wave speed. These waves emerge first as short periodic, near sinusoidal waves, in the inception region and may evolve into a highly irregular state over a long distance and time. As described by Chang [3] and reported by Oron and Gottlieb [4], a general scenario of formation and evolution of naturally excited waves consists of some main stages including: (i) downstream amplification of a disturbance to form a one humped wave, (ii) saturation of the wave to a finite amplitude structure, (iii) self organization of the pattern into lumped solitary waves, (iv) amplification of transverse disturbances to form an essentially three dimensional pattern. These stages were also observed in experiments by Gollub and co-workers [5–7]. In fact, the final pattern selection depends on the flow parameter set. For moderate Reynolds numbers,

* Corresponding author.
E-mail addresses: m_amaouche@yahoo.fr (M. Amaouche), nadbouam@yahoo.fr (N. Mehidi), amatousse@yahoo.fr (N. Amatousse).

0997-7546/$ – see front matter © 2004 Elsevier SAS. All rights reserved.
doi:10.1016/j.euromechflu.2004.06.001

the asymptotic state is dominated by long solitary waves regardless of initial disturbances. These solitary waves have many distinctive properties among which is the existence of a characteristic wavelength between solitary like pulses which is much larger than the film thickness. Kapitza and Kapitza [8] were the firsts to characterize the wave structure on the film surface; they reported the formation of two types of waves when pulsations are imparted at the inlet of a vertically falling water film. The first one is a wave train of nearly sinusoidal pattern produced by a small amplitude and high frequency forcing and which propagates downstream without changing their slope and speed appreciably. The second one is solitary waves which can be observed immediately without an incipient region, when the perturbing pulses are strong and less frequent. Liu and Gollub [6] observed that small amplitude sinusoidal waves at the entrance can evolve rapidly into solitary pulses (within 20 cm for a vertical film); the characteristics of the waves can increase downstream by nearly one order of magnitude after the transition to solitary pulses that subsequently destabilize up to developed space time chaos. In Liu et al. [5], unstable periodic waves were tracked until they developed spatially chaotic structure via subharmonic bifurcations and side band instability depending on the forcing frequency. The phenomenon of period doubling was also observed by Brauner and Maron [9] without artificial perturbations.

From a theoretical viewpoint, a great deal has also been learned about the onset of waves and their weakly nonlinear evolution since the works by Benjamin [10] and Yih [11]; They computed, by performing a long wavelength expansion of the Orr–Sommerfeld (OS) equation, neutral stability curve and found that the condition for the flat solution to be unstable is $R > \frac{5}{6}\cot\theta$. This means that at sufficiently large Reynolds number, the destabilizing effects of inertia overcome the stabilizing influence of gravity. It is worth noting that the critical condition does not involve the Weber number since the surface tension forces are negligible in the limit of large wavelength disturbances. It is also known [12,13] that the instability may manifest itself as relatively short shear waves for small gravity effects and sufficiently low surface tension. In this case, the critical Reynolds number is found to be a nonmonotonic function of θ and W. In order to determine the nature of interfacial instabilities, Brevdo et al. [14] have examined the dynamics of wave packets by solving the linearized Navier–Stokes equations for spatially localized disturbances; they showed that the flow over inclined planes is convectively unstable at least up to very large Reynolds numbers.

While linear analysis is a powerful tool to locate the bifurcation points as well as to predict qualitative characteristics of developing disturbances, it does not provide any quantitative information about the fully developed region far away from the inlet where nonlinearity dominates the wave system. In order to accurately describe certain special situations (as in, e.g., stationary states), the impact of nonlinearity must be considered. This can be achieved within the full Navier–Stokes (NS) equations. Unfortunately, these equations are not amenable to analytical investigations and their numerical integration in the presence of a moving boundary is a notoriously expensive task. For this, they are generally restricted to relatively small Reynolds numbers. For instance, finite elements were used by Bach and Villadsen [15] and by Kheshgi and Scriven [16] who found stationary solitary waves on a vertically falling film respectively in the range $2.5 < R < 25$ and for $R < 10$. The highly nonlinear character of the phenomena has also motivated several approaches: perturbative expansions, normal form analysis and boundary layer theories, all derived from the NS equations under certain assumptions.

The common feature of all these models is that by taking advantage of the smallness of certain parameters and by focusing on particular regimes, the dependence of the cross wise coordinate is eliminated, thereby providing a substantial simplification [17] of the problem. The first, the simplest and the most commonly used nonlinear model was derived by Benney [18] by introducing a long wave parameter μ to expand the full hydrodynamic equations, with the assumptions that R and $\mu^2 W$ are $\mathcal{O}(1)$. This led to the so called Benney equation (BE), which describes the film flow in terms of a single evolution equation for the free surface shape. Oron and Gottlieb [4] showed, by comparison with a direct numerical simulation of the basic equations, that the validity range of the BE is limited to a small vicinity of the critical Reynolds number. Its solution significantly deviates from the numerical one and developed a finite time singularity at some distance beyond the stability threshold despite the regularizing effect of the surface tension. This behavior was first noticed by Pumir et al. [19] and further studied by Rosenau et al. [20]. The long wave assumption allowed the derivation of other celebrated models like the Kuramoto–Sivashinsky equation [21], the Kawahara equation [22] and their variants as for instance the regularized model proposed by Ooshida [23]. Quite recently, Panga and Balakotaiah [24] proposed a new evolution equation by means of a suitable scaling allowing to introduce some correction terms that are missing in the long wave equations. Their solutions are, similarly to that of the BE, not satisfactory far from the onset of instability. The failure of these long wave models, based on a single evolution equation for the film depth, is partly due to their incapacity of capturing all of the inertia effects. For this a more realistic approach is needed to describe the film dynamics at moderate and high Reynolds numbers. Such approach is firstly proposed by Shkadov [25] by performing a depthwise integration of the momentum equation and assuming a self similar semi parabolic velocity profile. Even though the resulting model, termed the integral boundary layer (IBL) one, does not exhibit any divergence, it does not predict neither the stability threshold correctly, as the BE does, nor the Hopf bifurcation. Further developments of the IBL model were done by many authors. Nguyen and Balakotaiah [26] and Lee and Mei [27] retained more terms in the governing equations but kept the conventional parabolic velocity profile. Yu et al. [28] used a more general velocity profile than the parabolic one. Taking advantages of the numerical simulation of the linear stability problem, a new simple equation is proposed by Kliakhandler [29]. Ruyer-Quil and Manneville [30–32] derived several models by combining a long wave expansion and a Galerkin approximation using specific polynomials as test functions. This technique is based on the strong cross stream coherence of the flow ensured by

viscosity. Thus it allows to better capture the viscous effects which are dominant at small Reynolds numbers and thereby yields a correct condition for the onset of instability. The latter is retrieved even by using the first basic polynomial alone. On the other hand, even if these authors assume the inertia effects to be small compared to the viscous ones such that $R = \mathcal{O}(1)$ their studies show remarkable agreement with experiments and numerics up to quite large Reynolds number. Most of the previous studies are performed in the limit of large Weber number, neglecting the cross stream inertia effects. In situations where the latter are of comparable importance with the capillary effects such that $W = \mathcal{O}(1)$, the available results need to be improved. In these conditions, the long wave analysis remains applicable provided that the Reynolds number is large. Accordingly, large Reynolds numbers and Weber numbers of order unity will be considered in what follows. In many respects, our modeling strategy parallels the works by Lee and Mei [27] and Ruyer-Quil and Manneville [31,32]; it consists in expanding the velocity profile on some basis polynomials and using a refinement of the integral Polhausen–Von Karman averaging technique. The model still remains correct in the limit of large W allowing then to consider small and moderate Reynolds number so long as the product WR is large in order that the long wave analysis be ensured. In Section 2, we first recall the formulation of the problem in terms of its primary variables, namely the velocity field, the pressure and the free surface shape. A third order system is then obtained by applying the long wave expansion. The Galerkin procedure is outlined in Section 3 where four coupled equations are derived for the spatio temporal evolution of the fluid depth, the flow rate and two other relevant variables. The linear stability of these equations is carried out in Section 4; this leads to the dispersion relation from which the marginal stability curve is obtained. At marginality an unstable disturbance has the character of a wavepacket around the most unstable mode which moves at its group velocity and spreads while it grows. Of particular interest is the special case when the group and the phase velocities coincide. This happens under suitable conditions, when the squeeze due to nonlinearity is balanced exactly by the expansion due to the dispersion, leading to spatially localized waves that propagate with constant velocities and undistorded shapes. Looking for the limited but important class of these disturbances, allows to turn the set of partial differential equations into a dynamical system parametrized by their celerities. This question is examined in Section 5 by means of the simplest model resulting from a parabolic velocity profile. The problem is firstly converted into a three dimensional dynamical system with the film depth and its derivatives with respect to the comoved coordinate being the state variables; it appears as either a nonlinear eigenvalue problem when boundary conditions are prescribed at both upstream and downstream infinities or as an initial value problem when no downstream behavior is required for the traveling waves. Here, we are just interested in the latter case where the wave celerity, considered as a free parameter, plays a fundamental role. Some concluding remarks are finally given in the last section.

2. Problem statement

Consider a thin liquid film flowing down an inclined plane making an angle θ with the horizontal under the action of gravitational field $\mathbf{g}$ and surface tension σ. The fluid motion is referred to Cartesian coordinates system in which the x axis coincides with the inclined bottom from which the y coordinate is counted normally. A schematic drawing of the film flow is shown in Fig. 1. Denoting by $\Omega(t)$ the domain occupied at time t by the fluid, the governing equations are:

$$\mathbf{v}_t + (\mathbf{v}\cdot\nabla)\mathbf{v} = -\nabla p/\rho + \nu\nabla^2\mathbf{v} + \mathbf{g} \quad \text{in } \Omega(t), \tag{1}$$

$$\nabla\cdot\mathbf{v} = 0 \quad \text{in } \Omega(t), \tag{2}$$

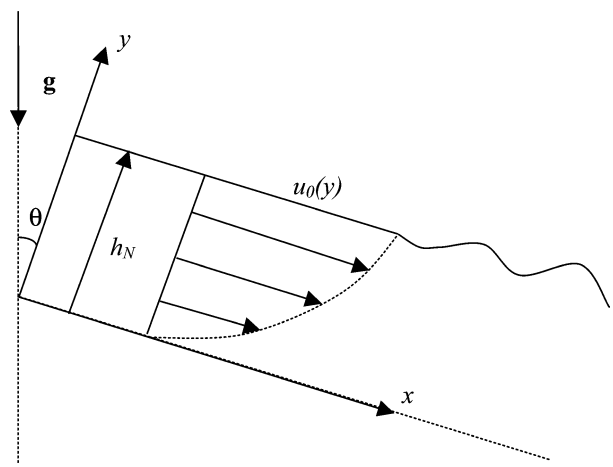

Fig. 1. Schematic picture of a film flowing down an inclined plane.

where $\mathbf{v} = (u, v)$ is the velocity field, ρ is density, p is the pressure, ν is the kinematic viscosity and $\Omega(t) = \{(x, y), x \in \Re, 0 < y < h(x, t)\}$; $h(x, t)$ is the local depth of the liquid layer. The above equations must be solved subject to:

– the no-slip condition at the bottom

$$\mathbf{v} = \mathbf{0} \quad \text{at } y = 0; \tag{3}$$

– the kinematic condition which states that the free surface is advected by the fluid

$$h_t + uh_x = v \quad \text{at } y = h(x, t); \tag{4}$$

– and the dynamic free surface condition which expresses the equilibrium of all forces acting on a unit area

$$\mathbf{T} \cdot \mathbf{n} + \sigma(\nabla \cdot \mathbf{n})\mathbf{n} = \mathbf{0} \quad \text{at } y = h(x, t), \tag{5}$$

where $\mathbf{T}$ is the stress tensor and $\mathbf{n}$ is the unit outward normal vector to the free boundary

$$\mathbf{n} \equiv (1, -h_x)(1 + h_x)^{-1/2}. \tag{6}$$

Subscripts denote partial derivatives. There exists a well-known time independent solution, referred as the Nusselt solution for the system of Eqs. (1)–(5). The Nusselt film thickness h_N is constant and the only nonzero component of velocity is the streamwise one. It only changes across the film and is given by: $u_0 = g\frac{\sin\theta}{\nu}(h_N y - y^2/2)$. The corresponding depth averaged velocity and flow rate are respectively $u_N = g\sin\theta h_N^2/3\nu$ and $q_N = h_N u_N$. Accordingly, only one of the two parameters, either q_N or h_N may be free, leading then to two physical situations. The stability of the Nusselt solution is being considered here within the long wave assumption. To this end, we first write all governing equations with normalized variables by using the following scaling factors: the streamwise coordinate x is scaled by a characteristic wavelength L and the normal coordinate y by the Nusselt film thickness. The velocity components u and v are referred to u_N and to μu_N respectively, μ being the longwave parameter h_N/L. The time and the pressure are in units of L/u_N and $\rho\nu u_N/\mu h_N$ respectively. After being simplified by dropping the terms that are of order μ^4 or higher, Eqs. (1), (2) acquire the following dimensionless form:

$$u_x + v_y = 0, \tag{7}$$

$$R\mu\frac{Du}{Dt} + p_x = 3 + \nabla_\mu^2 u, \tag{8}$$

$$R\mu^3\frac{Dv}{Dt} + p_y = -3\mu\cot\theta + \mu^2 v_{yy}. \tag{9}$$

The boundary conditions are:

– at the bottom:

$$u = v = 0; \tag{10}$$

– at the free surface:

$$v = h_t + uh_x, \tag{11}$$

$$u_y + \mu^2(v_x - 4u_x h_x) = 0, \tag{12}$$

$$p - 2\mu^2 v_y + RW\mu^3 h_{xx} = 0. \tag{13}$$

In the above, operators D/Dt and ∇_μ^2 indicates the total derivative with respect to the time and the normalized Laplace operator $\mu^2\partial_x^2 + \partial_y^2$, $R = u_N h_N/\nu$ and $W = \sigma/(\rho u_N^2 h_N)$ indicate the Reynolds and Weber numbers respectively. The Weber number is thus defined in terms of the ratio of the pressure drop due to surface tension σ/h_N and the dynamic pressure ρu_N^2. Another formulation of the Weber number exists comparing σ/h_N to the hydrostatic pressure drop $\rho g h_N \sin\theta$ across the fluid layer ($W' = \sigma/\rho g h_N^2 \sin\theta$) such that $W' = WR/3$. Integrating the incompressibility condition (7) over the film thickness and using the kinematic condition (11), one obtains:

$$q_x + h_t = 0, \tag{14}$$

where $q(x, t) = \int_0^h u\,\mathrm{d}y$ is the flow rate, one of the most important variable of the problem.

In the same way, the integration of the y momentum equation combined with the boundary condition (13) provides the pressure field;

$$p(x,y) = 3\mu(h-y)\cot\theta + R\mu^3\left[\int_y^h \frac{Dv}{Dt}\,\mathrm{d}y - Wh_{xx}\right] - \mu^2(u_x + u_x|_h). \tag{15}$$

Differentiating this equation with respect to x and using Eq. (8), yield:

$$u_{yy} + 3(1-\mu h_x\cot\theta) - R\mu\frac{Du}{Dt} + \mu^2\big(2u_{xx} + (u_x|_h)_x\big) + R\mu^3\left[Wh_{xxx} - \frac{\partial}{\partial x}\int_y^h \frac{Dv}{Dt}\,\mathrm{d}y\right] = 0, \tag{16}$$

where the pressure is eliminated and $v = -\int_0^y u_x\,\mathrm{d}y$. The previous system is thus reduced to the single equation (16) subject to the adhesion condition at $y=0$ together with the condition (12). The expression (15) shows that W compares the pressure induced by surface tension to the cross stream effects Dv/Dt. Therefore, the latter should be kept for consistency when $W = \mathcal{O}(1)$. On the other hand, $\mu^2 W'$ appears in Eq. (16) such that it compares the pressure gradient h_{xxx} generated by surface tension to the stream wise gravity force $3h_x\cot\theta$. The balance between these two effects is precisely the mechanism that generates the capillary-gravity waves preceding the wave front and that, consequently, prevents the wave from breaking. Therefore, the long wave expansion requires W' to be large. Situations can effectively be found where $W = \mathcal{O}(1)$ so that cross stream momentum terms Dv/Dt should be taken into account and W' sufficiently large for ensuring the long wave analysis. These situations correspond to large Reynolds numbers.

3. Method of solution

The velocity $u(x,y,t)$ is expanded in a self similar manner such that the boundary conditions are satisfied

$$u(x,y,t) = S_K(x,y,t) + a(x,t)\tilde{u}(\eta), \tag{17}$$

where $S_K(x,y,t) = \sum_{k=0}^{K} a_k(x,t)u_k(\eta)$, $\eta = y/h(x,t)$ and $u_k(\eta) = \eta^{k+1} - \frac{k+1}{k+2}\eta^{k+2}$.

We observe that $\frac{\partial u_k}{\partial\eta}|_1 = 0$; for this reason an appropriate term $a(x,t)\tilde{u}(\eta)$ is added to the series $S_K(x,y,t)$ to take into account the deviation of the velocity profile induced by the nonuniform condition (12). The polynomial expansion is truncated to some sufficiently high order K to insure resolution of effects due to steep gradients. The polynomial $\tilde{u}(\eta)$ will be specified later and a Galerkin projection will be used to determine the equations for coefficients a_k. Before all, it is to be noted that the crudest approximation is with $K=0$ and $a=0$, which reduces to the parabolic model. The particular case $a_0 =$ constant gives the flat solution. Coefficients a_k, $k \geqslant 1$, emerge owing to the deformation of the free surface. As a result, it can be shown by successive differentiation of (16) with respect to y that these coefficients are at least of one order in μ. This property is turned to account by rewriting (17) in the form:

$$u(x,y,t) = u^{(0)} + \mu u^{(1)} + \mu^2 u^{(2)}. \tag{18}$$

It can be shown from (16) that $u^{(1)}$is at most a sixth order polynomial since $u^{(0)}$ is a second order one; this means that $u^{(1)}$ is determined by at most four fields $a_1,\ldots,a_4$. In fact, Ruyer-Quil and Manneville [31,32] showed that only two fields, say a_1 and a_2 are required to describe the first order correction $u^{(1)}$. The two other coefficients, a_3 and a_4 are enslaved to a_1 and a_2. Indeed, by neglecting second order terms in Eq. (16), one obtains:

$$\left.\frac{\partial^n u^{(1)}}{\partial y^n}\right|_h = R\mu\left(\frac{\partial}{\partial t} + u|_h\frac{\partial}{\partial x}\right)\left.\frac{\partial^{n-2}u^{(1)}}{\partial y^{n-2}}\right|_h, \quad n=3,5, \tag{19}$$

which gives:

$$\left.\frac{\partial^3 u^{(1)}}{\partial y^3}\right|_h = \left.\frac{\partial^5 u^{(1)}}{\partial y^5}\right|_h = 0 \quad \text{given that} \quad \left.\frac{\partial u^{(1)}}{\partial y}\right|_h = 0. \tag{20}$$

Taking this into account, the correction $u^{(1)}$may be written:

$$u^{(1)} = a_1\tilde{u}_1 + a_2\tilde{u}_2, \tag{21}$$

where $\tilde{u}_1$and $\tilde{u}_2$ are linear combinations of (u_1, u_2) and (u_1, u_3, u_4) respectively; hence:

$$\left.\frac{\partial^n \tilde{u}_1}{\partial y^n}\right|_h = 0, \quad \left.\frac{\partial^n \tilde{u}_2}{\partial y^n}\right|_h = 0, \quad n=1,3,5. \tag{22}$$

Notice that, by the implicit notational change introduced by (18), the coefficients a_1 and a_2 are accordingly of zeroth order in μ. Now, let us examine the second order correction $u^{(2)}$. First of all we notice that it is at most a tenth order polynomial since the second order inertia term is a polynomial of degree eight resulting from the interaction between zeroth and first order solutions. Hence, $u^{(2)}$ may be written as follows:

$$u^{(2)} = b_0 u_0 + \cdots + b_8 u_8 + a\tilde{u}, \tag{23}$$

where $\tilde{u}$ is an additive polynomial such that:

$$\left.\frac{\partial \tilde{u}}{\partial \eta}\right|_{\eta=1} = 1. \tag{24}$$

Requiring the fulfillment of (12) and taking advantage of (24), one finds:

$$a = h\big(4u_x^{(0)} h_x - v_x^{(0)}\big). \tag{25}$$

This means that nine fields $b_0, \ldots, b_8$ are a priori required to describe the correction $u^{(2)}$. In fact, this number can be reduced by examining the successive odd derivatives of $u^{(2)}$, with respect to y, evaluated at the free surface. To this end, we begin by differentiating (16) with respect to y. Ignoring third order terms yields:

$$\left.\frac{\partial^3 u}{\partial y^3}\right|_h = R\mu\left(\frac{\partial}{\partial t} + u|_h \frac{\partial}{\partial x}\right) - \left.\frac{\partial u}{\partial y}\right|_h - 2\mu^2 \left.\frac{\partial u_{xx}}{\partial y}\right|_h \tag{26}$$

which, owing to the boundary condition (12), and removing again third order terms give:

$$\left.\frac{\partial^3 u^{(2)}}{\partial y^3}\right|_h = -2\left.\frac{\partial u_{xx}^{(0)}}{\partial y}\right|_h. \tag{27}$$

This condition finally reads:

$$\left.\frac{\partial^3 u^{(2)}}{\partial y^3}\right|_h = 2\frac{a_0}{h^3}\big(4h_x^2 - hh_{xx}\big) - 4a_{0x}\frac{h_x}{h^2}. \tag{28}$$

Pursuing the differentiation of (16) and continuing to ignore third order terms, we are led to:

$$\left.\frac{\partial^{2n+1} u^{(2)}}{\partial y^{2n+1}}\right|_h = 0, \quad n = 2, 3, 4. \tag{29}$$

This means that, when evaluated at the free surface, the fifth, seventh and ninth derivatives of the second order correction are equal to zero. The constraints (29) together with (28) allow to reduce to only five the number of independent coefficients in the sequence $b_0, \ldots, b_8$. So (23) becomes:

$$u^{(2)} = b_0^* u_0^* + \cdots + b_4^* u_4^* + a\tilde{u}, \tag{30}$$

where $u_0^* = u_0$, $u_1^*, \ldots, u_4^*$ are linear combinations of (u_1, u_2), (u_1, u_3, u_4), (u_1, u_3, u_5, u_6), $(u_1, u_3, u_5, u_7, u_8)$ respectively. Thus, a full third order theory would require the use of all the fields $b_0^*, \ldots, b_4^*$ in addition to the unknown a_0, a_1, a_2 and h. However, in order to reduce the analysis we will restrict our attention to a relatively simple approximation which consists in representing $u^{(2)}$ by the sole term $a\tilde{u}$ in (30). The calculation becomes then straightforward and essentially the same as in the second order theory since the truncation avoids precisely the introduction of additive fields. Besides the great simplification this truncation provides, the main advantage it also presents is its ability to accurately describe the instability threshold by properly choosing the polynomial $\tilde{u}$. Before doing this, we first substitute to the basis u_k an orthogonal one, in the sense of $L^2(0, 1)$. The basic idea dictating the choice of the latter, noted g_k, is identical to that for the second order theory, i.e., in order to conveniently implement the Galerkin procedure. Thence, we will write u in the form:

$$u = a_0 g_0 + \mu(\tilde{a}_1 g_1 + \tilde{a}_2 g_2) + \mu^2 a(\eta + g_3), \tag{31}$$

where

$$\begin{aligned} g_0(\eta) &= \eta - \frac{1}{2}\eta^2, \qquad g_1(\eta) = \eta - \frac{17}{6}\eta^2 + \frac{7}{3}\eta^3 - \frac{7}{12}\eta^4, \\ g_2(\eta) &= \eta - \frac{13}{2}\eta^2 + \frac{57}{4}\eta^3 - \frac{111}{8}\eta^4 + \frac{99}{13}\eta^5 - \frac{33}{32}\eta^6, \end{aligned} \tag{32}$$

g_3 is a polynomial of degree eight such that $\frac{\partial g_3}{\partial \eta}|_{\eta=1} = 0$; so it may be put in the form:

$$g_3 = \alpha_0 g_0 + \alpha_1 g_1 + \alpha_2 g_2 + \alpha u_6. \tag{33}$$

Using orthogonality of $g_3+\eta$ to the subspace spanned by g_0, g_1 and g_2 allows to eliminate α_0, α_1 and α_2 in favor of α and defines g_3 as a one parameter family of polynomials of degree eight.

$$g_3(\eta)=-\left(\frac{53}{528}\alpha+\frac{25}{13}\right)g_0(\eta)+\left(\frac{9}{26}\alpha+\frac{9}{8}\right)g_1(\eta)-\left(\frac{113}{192}\alpha+\frac{299}{256}\right)g_2(\eta)+\alpha\left(\eta^7-\frac{7}{8}\eta^8\right). \tag{34}$$

The optimal value of α which generally does not provide the simplest polynomial will be specified later from the numerical tests. Instead of the fields a_0, $\tilde{a}_1$ and $\tilde{a}_2$ without direct physical meaning, we introduce the flow rate and its corrections noted s_1 and s_2 by the following transformation [31]:

$$a_0=3\frac{q-s_1-s_2}{h},\qquad \tilde{a}_1=45\frac{s_1}{h},\qquad \tilde{a}_2=210\frac{s_2}{h}. \tag{35}$$

Now, we apply the Galerkin weighted residual procedure to (16). Then requiring the orthogonality of the residual to the basis functions g_0, g_1 and g_2, one successively obtains:

$$q_t-s_{1t}-s_{2t}+Q_1(q,h,s_1,s_2)+\mu^3\widetilde{Q}_1(q,h,s_1,s_2)=0, \tag{36}$$

$$s_{1t}+S_1(q,h,s_1,s_2)+\mu^3\widetilde{S}_1(q,h,s_1,s_2)=0, \tag{37}$$

$$s_{2t}+S_2(q,h,s_1,s_2)+\mu^3\widetilde{S}_2(q,h,s_1,s_2)=0. \tag{38}$$

The first equation can be rewritten in a more convenient form by eliminating s_{1t} and s_{2t}; this gives:

$$q_t+Q_2(q,h,s_1,s_2)+\mu^3\widetilde{Q}_2(q,h,s_1,s_2)=0. \tag{39}$$

$(Q_1,\ldots,\widetilde{Q}_2)$ are differential operators; their explicit form is omitted here and given in the appendix owing to their excessive length. Eqs. (37)–(39) are naturally completed by the conservation equation of the flow rate (14). We note that $\widetilde{Q}_2$, $\widetilde{S}_1$ and $\widetilde{S}_2$ involve corrections due to inertia terms in proportion with μ^3. Neglecting these terms and performing the transformation $(t,q,s_1,s_2,R,W)\to(\frac{1}{3}t,3q,3s_1,3s_2,\frac{1}{3}R,9\Gamma)$ on Eqs. (37)–(39) allow to recover Eqs. (11)–(13) given in [32]. Let us now examine the implications, on the linear stability of the flat solution, of these additive inertia terms whose relevance is obvious when working with large Reynolds numbers.

4. Linear stability results

We further consider the stability of the basic flow against two dimensional small disturbances. Linear stability analysis is useful to determine the most unstable mode, to locate the onset of instability in the parameter space as well as to predict qualitative characteristics of developing perturbations. If we assume that the free surface is weakly deformed, i.e., $(q,h,s_1,s_2)=(1,1,0,0)+(\tilde{q},\tilde{h},s_1,s_2)$ with $|\tilde{q}|,|\tilde{h}|,|s_1|$ and $|s_2|\ll 1$, the foregoing set of equations can be linearized. Therefore the normal mode representation that consists in seeking the disturbances in the wave like form, i.e., proportional to $\mathrm{e}^{\mathrm{i}(kx-\omega t)}$, can be applied. The exponents ω and k are complex; their imaginary part describes the temporal and spatial growth rate of the disturbances while their real part gives the wavenumber and the frequency of the disturbances. The condition for a nontrivial solution to exist is that ω and k must satisfy a dispersion relation we put in the form:

$$\sum_{j=0}^{8}A_jk^j=0 \tag{40}$$

with:

$$A_0=-\frac{5}{2}\mathrm{i}\omega-\frac{15}{13}R\omega^2+\frac{25}{429}\mathrm{i}R^2\omega^3+\frac{2}{3861}R^3\omega^4,$$

$$A_1=\frac{15}{2}\mathrm{i}+\frac{435}{143}R\omega-\frac{245}{1287}\mathrm{i}R^2\omega^2-\frac{2}{1001}R^3\omega^3,$$

$$A_2=\frac{5}{2}\cot\theta-\frac{249}{143}R+\left(-\frac{9}{2}-\frac{2}{13}R\cot\theta+\frac{7340}{39039}R^2\right)\mathrm{i}\omega+\left(-\frac{359}{1456}R-\frac{3}{2002}R^2\cot\theta+\frac{34}{13013}R^3\right)\omega^2$$
$$+\frac{2027}{864864}\mathrm{i}R^2\omega^3+\varepsilon\left[-\frac{4}{13}\mathrm{i}\omega-\frac{4727}{16016}R\omega^2+\frac{2209}{144144}\mathrm{i}R^2\omega^3+\left(\frac{773}{5765760}-\frac{4567}{11130799680}\alpha\right)R^3\omega^4\right],$$

$$A_3=\left(6+\frac{152}{1001}R\cot\theta-\frac{684}{13013}R^2\right)\mathrm{i}+\left(\frac{12205}{24024}R+\frac{8}{3003}R^2\cot\theta-\frac{184}{143143}R^3\right)\omega-\frac{3439}{524160}\mathrm{i}R^2\omega^2$$

$$+\varepsilon\left[\frac{12}{13}\mathrm{i}+\frac{2512}{3003}R\omega-\left(\frac{9041}{144144}+\frac{132443}{3710266560}\alpha\right)\mathrm{i}R^2\omega^2+\left(-\frac{23479}{34594560}+\frac{5121049}{2018385008640}\alpha\right)R^3\omega^3\right],$$

$$A_4=\frac{5}{6}WR-\frac{30993}{128128}R-\frac{74}{65065}R^2\cot\theta+\frac{24}{143143}R^3+\left(-\frac{2}{39}W+\frac{4591}{780780}\right)\mathrm{i}R^2\omega-\frac{1}{2002}WR^3\omega^2$$
$$+\varepsilon\left[-\frac{71601}{128128}R+\frac{4}{13}\cot\theta-\frac{72595}{219648}\mathrm{i}\omega-\frac{6}{1001}\mathrm{i}R\omega\cot\theta+\left(\frac{108579}{1281280}+\frac{14392471}{96113571840}\alpha\right)\mathrm{i}R^2\omega\right.$$
$$-\left(\frac{217799}{5031936}+\frac{4567}{51397632}\alpha\right)R\omega^2+\left(\frac{24827783}{19788088320}-\frac{4998239}{807354003456}\alpha\right)R^3\omega^2$$
$$\left.+\left(\frac{1445}{2306304}+\frac{4567}{8904639744}\alpha\right)\mathrm{i}R^2\omega^3\right],$$

$$A_5=\frac{152}{3003}W\mathrm{i}R^2-\frac{1773}{1041040}\mathrm{i}R^2+\frac{8}{9009}WR^3\omega+\varepsilon\left[\frac{406907}{878592}\mathrm{i}+\frac{13}{3003}\mathrm{i}R\cot\theta\right.$$
$$-\left(\frac{16655}{439296}+\frac{150869}{1045524480}\alpha\right)\mathrm{i}R^2+\left(\frac{4552231}{36900864}+\frac{3032121773}{6458832027648}\alpha\right)R\omega$$
$$\left.+\left(-\frac{136693}{137417280}+\frac{408517}{54664593984}\alpha\right)R^3\omega-\left(\frac{4517441}{1798917120}+\frac{190633537}{104956020449280}\alpha\right)\mathrm{i}R^2\omega^2\right],$$

$$A_6=-\frac{74}{195195}WR^3+\varepsilon\left[\frac{4}{39}WR+\frac{6}{1001}\cot\theta-\left(\frac{9167299}{105431040}+\frac{2171260541}{4305888018432}\alpha\right)R\right.$$
$$+\left(\frac{386041}{1374172800}-\frac{182999}{48590750208}\alpha\right)R^3-\frac{2}{1001}W\mathrm{i}R^2\omega-\frac{2573}{494208}\mathrm{i}\omega$$
$$\left.+\left(\frac{25873069}{7915235328}+\frac{2261602009}{4618064899768320}\alpha\right)\mathrm{i}R^2\omega-\left(\frac{4133}{5765760}+\frac{4567}{1712430720}\alpha\right)R\omega^2\right],$$

$$A_7=\varepsilon\left[\frac{13}{9009}W\mathrm{i}R^2+\frac{8363}{1153152}\mathrm{i}+\left(-\frac{28982399}{21107294208}+\frac{4991070473}{3078709933178880}\alpha\right)\mathrm{i}R^2\right.$$
$$\left.+\left(\frac{118721}{54512640}+\frac{32575837}{2498952867840}\alpha\right)R\omega\right],$$

$$A_8=\varepsilon\left[\frac{2}{1001}WR-\left(\frac{217361}{133253120}+\frac{474156721}{34985340149760}\alpha\right)R\right].$$

Notice that the parameter μ is dropped by rescaling the streamwise coordinate and ε $(=1)$ is introduced to locate the terms proportional to μ^3. For easier comparison with previous results, e.g., those in [32], the velocity u must be rescaled by the velocity at the interface. Accordingly, the transformation $(\omega, R, W)\to(\frac{3}{2}\omega, \frac{2}{3}R, \frac{9}{2}W/R)$is required. Then, comparison of (40) with the relation (19) given in [32] shows that all the terms are identical, except those involving the factor ε. The marginal state is obtained from (40) by setting $\mathrm{Im}\,\omega=\mathrm{Im}\,k=0$. Then, splitting the result into real and imaginary parts, yields two expressions for the marginal wave frequency ω_m and wavenumber k_m we formally write in the form:

$$F_1\left(\omega_m, k_m, R, W, \frac{\cot\theta}{R}\right)=0, \tag{41}$$

$$F_2\left(\omega_m, k_m, R, W, \frac{\cot\theta}{R}\right)=0. \tag{42}$$

Eliminating ω_m from these equations allows to express the marginal wave number k_m as function of the relevant parameters. The critical conditions for the onset of instability are then obtained: $\omega_c=k_c=0$, $R_c=\frac{5}{6}\cot\theta$ and the critical wave celerity is $c_0=3$. All disturbances are stable for $R<R_c$ and for $R>R_c$ a marginal curve exists which separates the damped eigenmodes $(k>k_m)$ from the unstable ones $(k<k_m)$. At marginality, the spatial and temporal modes coincide and the spatial growth of a mode is related to the temporal growth by the group velocity $(c_g)_m=(\partial(\mathrm{Re}\,\omega)/\partial(\mathrm{Re}\,k))_m$ not the phase velocity $(c_m=\omega_m/k_m)$. On assuming that the dispersion relation (40) gives ω as an analytic function of k, the Cauchy–Riemann conditions yield along the marginal curve:

$$(c_g)_m=\mathrm{Re}(\mathrm{d}\omega/\mathrm{d}k)_m. \tag{43}$$

It is relevant to mention here that these two velocities are equal in the more restrictive case where the modes are of the traveling wave type. Beyond criticality $(R>R_c)$, a disturbance has the character of a wavepacket, around the most unstable mode, which moves at its group velocity. It spreads while its amplitude grows to a size sufficient to excite nonlinear interactions

between the other components; these interactions then retard the exponential growth until, finally, a new flow sets in. In view of the comparison to be made with the asymptotic solution of the OS equation, let us consider the temporal stability (i.e., k is real and ω is complex) near criticality. Then, expanding ω in powers of k and performing the notational changes $(\omega, R, W) \to (3\omega, R/3, 9W/R)$ in the dispersion equation (40) yields:

$$\omega = k + \left(\frac{2}{5}R - \frac{1}{3}\cot\theta\right)\mathrm{i}k^2 + \left(\frac{10}{21}R\cot\theta - \frac{4}{7}R^2 - 1\right)k^3 + \left(-\frac{1}{3}W + \frac{3}{5}\cot\theta - \frac{2}{15}R(\cot\theta)^2 + \frac{17363}{17325}R^2\cot\theta - \frac{471}{224}R - \frac{75872}{75075}R^3\right)\mathrm{i}k^4 + \mathcal{O}(k^5). \tag{44}$$

This equation is nothing but the exact asymptotic expansion of the OS equation that may be found in [30] (Eq. (88)). We further observe that the parameter α does not appear at the considered order in k. Let us introduce for convenience the Kapitza number ($Ka = \sigma/\rho g^{1/3}\nu^{4/3}$) which is constant for a given fluid. Expressed in terms of R and W, Ka becomes:

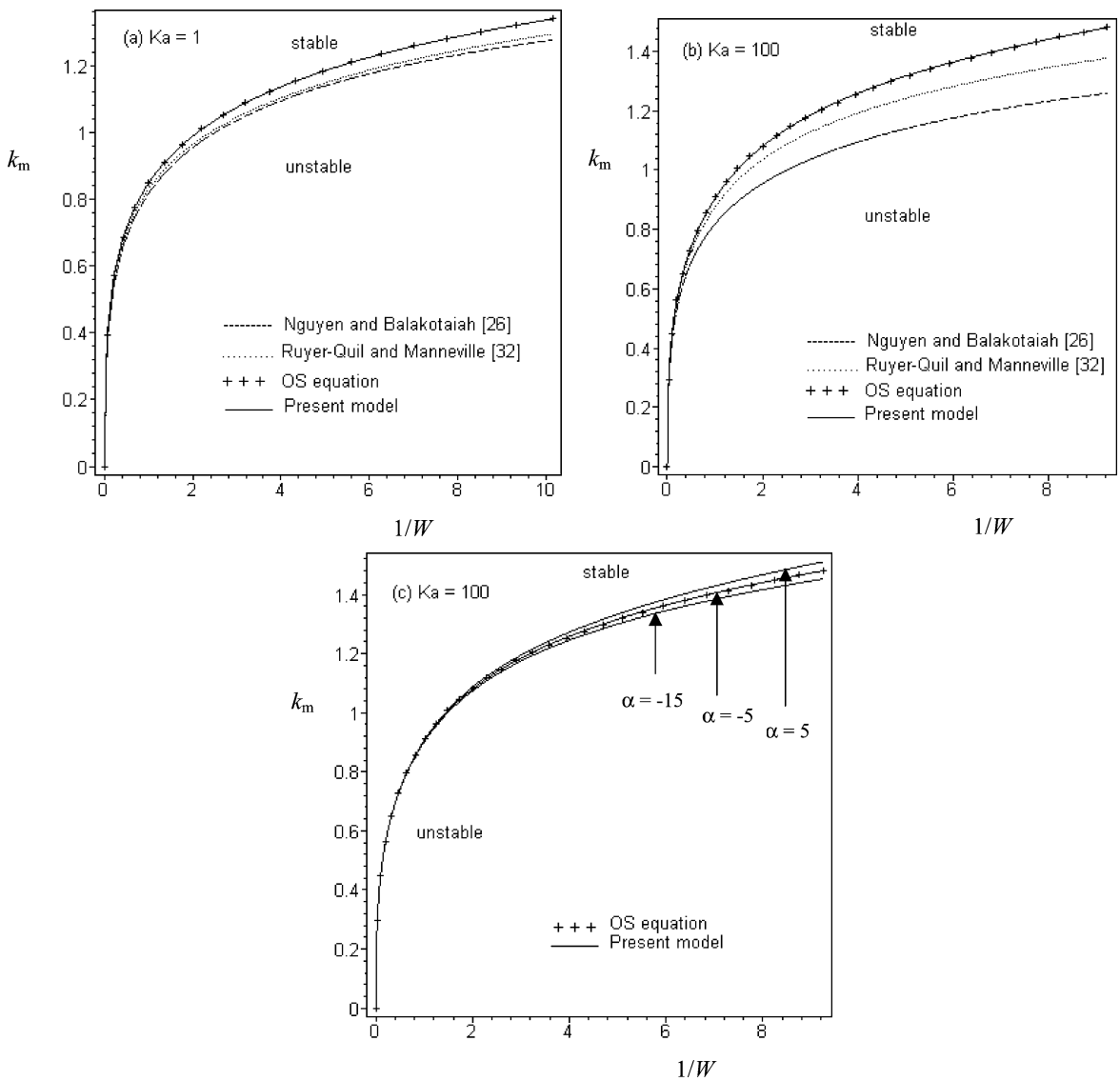

Fig. 2. Marginal stability curves for the Nusselt flow on a vertical plane. The marginal wavenumber is plotted against the inverse of the Weber number for two fluids characterized by their Kapitza number: (a) $Ka = 1$, (b) $Ka = 100$. The model follows quite closely the OS equation for a suitable choice of the parameter α ($\alpha = 1$ for $Ka = 1$ and $\alpha = -5$ for $Ka = 100$) (c) indicates the effects of varying α in the case $Ka = 100$.

$Ka = W(R^5/3)^{1/3}$. Recall that we are primarily interested with the particular situations of large R and $W = \mathcal{O}(1)$, which correspond to large Ka. Small Kapitza numbers corresponding to small R (therefore W must be large) are also considered for comparison. Fig. 2 shows neutral stability curves obtained from the present model, some recent ones and from the OS equation for various fluids in the case of vertical plane. It is clearly indicated that the models are all in good agreement with the OS equation at large W corresponding to viscous dominated regimes. We observe that the present model follows quite closely the OS equation whereas the other models diverge as W decreases, i.e., when inertia increases. This agreement is achieved owing to suitable choice of the parameter α, depending on the Kapitza number. Changing α significantly affects the neutral stability curve for large Ka. This can be illustrated through Fig. 2(c) where neutral stability curves corresponding to various α are compared to that given by the OS equation for $Ka = 100$; in this case, the best value of α (α_{opt}) is around -5. This value is selected in order that the maximum departure between the calculated value of k_m and that given by the OS equation does not exceed 10^{-3}. For $Ka = 1000$ numerical tests give, within the same accuracy, $\alpha_{\text{opt}} \simeq -2$. In the range of small Ka, the marginal wave number is found to be relatively insensitive to changes in the value of this parameter. For example, it is found that $\alpha_{\text{opt}} \in (-2, 1)$ for $Ka = 10$ and the influence of α is not discernible at all in the case of $Ka = 1$ provided that α is in the range $(-100, 100)$. This means that, the relevance of the parameter α which is introduced in order to improve the flexibility of the velocity profile especially appears when inertia effects are important.

5. A simplified model

The model described above by Eqs. (37)–(39) is too cumbersome and hardly tractable in the nonlinear case; this limits its practical usefulness. It is then advisable to abandon it in favor of an appropriate simplified version which takes advantage of some relevant terms originate from higher inertia effects. A great simplification can be obtained by a direct adiabatic elimination of the corrections s_1 and s_2 in Eq. (36). This consists in neglecting the temporal and spatial derivatives of s_1 and s_2, and assuming that the products of s_1 and s_2 with the derivatives of q or h can also be neglected. This simplification was introduced by Ruyer-Quil and Manneville [31,32] and in order to legitimate it, they argued that the relaxation times of s_1 and s_2 are much shorter than that of the flow rate. Using these assumptions, Eq. (36) yields the following simplified equation:

$$\frac{q}{h^2} - h + \frac{2}{5}Rq_t + \frac{34}{35}\frac{Rqq_x}{h} + hh_x\cot\theta - \frac{18}{35}\frac{Rq^2h_x}{h^2} + \frac{9}{5}\frac{h_xq_x}{h} - \frac{8}{5}\frac{h_x^2q}{h} + \frac{12}{5}\frac{h_{xx}q}{h} - \frac{9}{5}q_{xx} - \frac{1}{3}RhWh_{xxx}$$
$$+ \varepsilon R\left[\frac{23}{336}\frac{q^2h_x^3}{h^2} - \frac{11}{140}hq_{xt}h_x - \frac{187}{3360}qq_{xx}h_x + \frac{4633}{6720}qq_xh_{xx} - \frac{601}{2520}hqq_{xxx} - \frac{683}{2520}hq_xq_{xx} + \frac{107}{840}hq_th_{xx}\right.$$

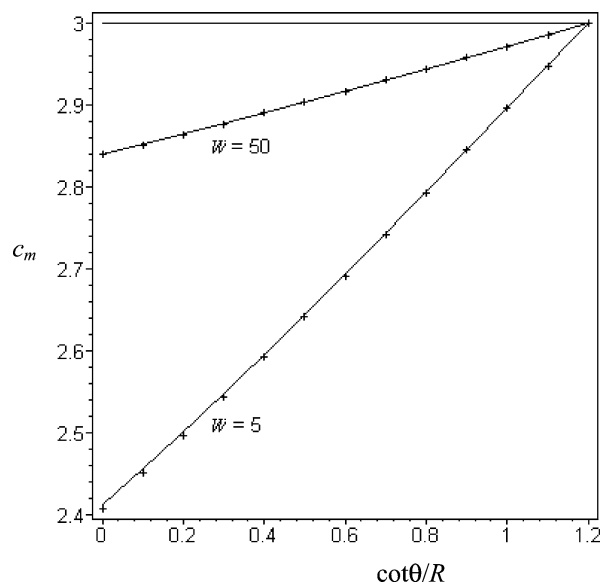

Fig. 3. Marginal stability curves against disturbances of traveling wave type. The marginal wave celerity c_m is given as a function of $\cot\theta/R$ for $W = 5$ and $W = 50$. This illustrates the accuracy of the simplified model (+) compared to the complete model (—).

$$+\frac{29}{140}q_t h_x^2+\frac{509}{1680}q_x^2 h_x-\frac{253}{1680}\frac{qq_x h_x^2}{h}-\frac{11}{140}h^2 q_{xxt}+\frac{241}{1344}q^2 h_{xxx}-\frac{111}{448}\frac{q^2 h_{xx}h_x}{h}\Bigg]=0. \tag{45}$$

It is to be noted that this equation can also be obtained in a roundabout way by combining the three equations (37)–(39). Eqs. (37) and (38) serve to express the enslavement of s_1 and s_2 to q and h. Their elimination from Eq. (39) then allows to get Eq. (45). The performance of this model is illustrated through Fig. 3 where are compared the restriction (to disturbances of traveling wave type) of its marginal stability curve and that resulting from the complete dispersion relation (40). Let us recall that for this type of disturbances, the group and phase velocities coincide. Equating them and making use of (43) result in a relation of the form:

$$f\left(R, W, \frac{\cot\theta}{R}\right)=0. \tag{46}$$

Then, eliminating R in favor of W and $(\cot\theta)/R$ allows to express c_m as a function of W (or Ka) and $(\cot\theta)/R$ in the linear instability region. Fig. 3 shows that there is a good agreement between the two models. As one would expect, greater is the Weber number (or Ka) better is the approximation.

6. Traveling wave solutions

In this section, our main interest focuses on studying the asymptotic form of the fully developed state. To this end, we consider a particular type of wave form that is steady in a moving frame, i.e., that travels at a constant celerity c without changing its shape. This type of solutions which are characterized by their celerity exists under suitable conditions, when the widening due to dispersion is balanced exactly by the narrowing effect due to the nonlinearity. Changing the parameter c in some range allows to explore the entire spectrum of asymptotic behavior of these traveling waves. For convenience we introduce the phase variable $\xi = x - ct$ to convert the two equations (14) and (45) into a three dimensional dynamical system. To this end, let us integrate Eq. (14) once, we obtain $q = q_0 + ch$ with q_0 being the integration constant which physically represents the flow rate in the comoved frame. Requiring the condition that the Nusselt flow must be solution for all c allows to express the flow rate in terms of flow depth and wave celerity. Since $q = 1$ for $h = 1$ (because of our scaling), one obtain:

$$q = 1 + c(h-1). \tag{47}$$

Therefore, eliminating q in favor of h, Eq. (45) can be written in a general compact vector form:

$$\frac{\mathrm{d}\mathbf{H}}{\mathrm{d}\xi}=\mathbf{F}(\mathbf{H},\mathbf{P}) \tag{48}$$

where $\mathbf{H}=(h, h_\xi, h_{\xi\xi})^t$ is the state variable vector, $\mathbf{P}=(W, R, c, \cot\theta)$ is the 4-dimensional vector of parameters and $\mathbf{F}=(h_\xi, h_{\xi\xi}, f/\delta)^t$ is the corresponding right-hand side vector with

$$\delta\equiv\delta(h)=Wh^3-\frac{391}{6720}h^4c^2+\frac{173}{480}h^3c(c-1)-\frac{241}{448}h^2(c-1)^2 \tag{49}$$

$$\begin{aligned} f=&\frac{3}{R}(1-h)(h^2+h+1-c)+h_\xi^3\left(\frac{23}{112}(c-1)^2+\frac{23}{560}hc(c-1)+\frac{23}{560}h^2c^2\right)\\ &+h_\xi^2\left(\frac{24}{5R}(c-1)+\frac{3}{5R}ch\right)+h_\xi\left(3h^3\frac{\cot\theta}{R}-\frac{54}{35}(c-1)^2+\frac{6}{35}hc(c-1)+\frac{6}{35}h^2c^2\right)\\ &+h_{\xi\xi}\left(\frac{9}{5R}h^2c-\frac{36}{5R}h(c-1)+h_\xi\left(-\frac{333}{448}h(c-1)^2-\frac{929}{2240}h^2c(c-1)+\frac{667}{3360}h^3c^2\right)\right). \end{aligned} \tag{50}$$

It is worth noting that:

(i) in addition to the trivial fixed point $\mathbf{H}_1=(1,0,0)$, the stationary wave solution exhibits another fixed point $\mathbf{H}_2=(\frac{1}{2}\{(4c-3)^{1/2}-1\},0,0)$ which does really exist only for $c>1$; it can only be viewed as an asymptotic part of a localized disturbance of hydraulic jump type propagating with a celerity c.

(ii) solving the system (48) therefore requires to specify the asymptotic conditions as $|\xi|\to\infty$, which may for instance correspond to either one or the other fixed point. In fact, it will be seen below that a suitable scaling transformation allows us to fix, without loss of generality, the Nusselt solution at upstream infinity.

(iii) when conditions are prescribed at both upstream and downstream infinities, we are led to a nonlinear eigenvalue problem with the eigenvalue c that has to be found together with the traveling solitary waves describing the thickness profile. In order that this type of solution (solitary waves) occurs, the set of parameters must satisfy some eigenrelation.

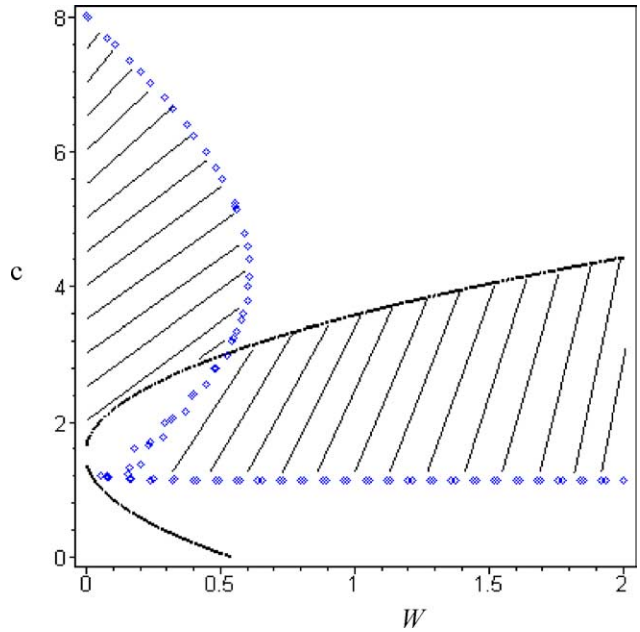

Fig. 4. Singular lines corresponding to the vanishing of the denominator δ given by (49) in the c versus W plane. $\delta(H_1) = 0$ (-), $\delta(H_2) = 0$ ($\diamond$). Heteroclinic orbits can only occur in hatched regions where none of the singularities intrude between the two fixed points.

(iv) on the other hand, the problem also may be considered as an initial value problem by prescribing only upstream conditions. In this context, the downstream behavior is not fixed in advance and become a result that depend on the wave celerity. Therefore the later may be viewed as a bifurcation parameter for a given set of other physical parameters, since c alone determines the second fixed point.

By varying the parameter c, the two solution branches intersect each other at the critical value $c = 3$; this suggests the possibility for the two fixed points to exchange here their stability. Before discussing the stability properties of these fixed points in the parameters space, it is interesting to first examine the singularities of the system (48); these correspond to the annulation of the denominator δ given by the expression (49). Thus, one obtains two singular thicknesses depending only on the Weber number and the bifurcation parameter c.

$$(H_S)\mp = \frac{[3360W + 1211c(c-1)] \mp 8[W(176400W + 127155c(c-1)) + 829c^2(c-1)^2]^{1/2}}{391c^2}. \tag{51}$$

Of course, this kind of breakdown does not occur in practice. Rather, the occurrence of the breakdown must be understood as a defect of third order models incorporating cross stream effects. Mei and Lee [27] pointed out that this could be cured by improving the long wave like approximation. For instance, adding fourth order terms these authors found that the singularity occurs either for a dry bed or for $c < 1$ in which case the conjugate fixed point does not exist. In order to a heteroclinic orbit connecting the two fixed points can exist, there must be no singularity between them; this means that a smooth transition corresponding to a transcritical bifurcation from the upstream fixed point to the downstream one can happen in these conditions by varying W and c. Fig. 4 shows in the W versus c plane, two shaded regions where none of the singular heights intrude between H_1 and H_2. The boundaries of these regions are constituted by the trajectories $\delta(H_1) = 0$ and $\delta(H_2) = 0$.

6.1. Stability and bifurcations of the fixed points

The dynamical system (48) is now considered to locate regions of the parameter space in which periodic and chaotic motion may occur. In principle, the full investigation of the underlying dynamics requires a numerical study of the model, due to its nonlinearity, but some insights about the behavior of the flow may be obtained from the linear analysis near the fixed points. We notice that the latter may however be restricted to only the stability properties of the upstream fixed point and therefore to the solutions bifurcating from it owing to the invariance of the system to the rescaling transformation $(\xi, h, c, R, W) \to (H_2\xi, H_2h, H_2^2c, R/H_2^3, WH_2^5)$. Hence, limiting ourselves to the study of the upstream fixed point, and following the usual method for solving sets of first order linear differential equations, trial solutions of the form $h \sim \exp(\lambda\xi)$

may be substituted into the equations. The conditions for a nontrivial solution to exist is that λ must be an eigenvalue of the Jacobian matrix and therefore must satisfies the cubic characteristic equation:

$$\lambda^3 + \left[\frac{\beta_1}{R}\lambda^2 + \beta_2\lambda + \frac{\beta_3}{R}\right] \Big/ \delta(1) = 0, \tag{52}$$

where the β coefficients are given by the following expressions:

$$\begin{aligned} \beta_1 &= -\frac{36}{5} + \frac{27}{5}c, \\ \beta_2 &= -3\frac{\cot\theta}{R} + \frac{6}{5}c^2 - \frac{102}{35}c + \frac{54}{35}, \\ \beta_3 &= 3(3-c). \end{aligned} \tag{53}$$

A topological singularity associated with an instability occurs when one real eigenvalue or two complex conjugated eigenvalues for the generic case (more for nongeneric case) cross the imaginary axis. In the case of real eigenvalue crossing; the generic bifurcation is the transcritical bifurcation; the two fixed points collapse at the critical value $c = 3$ for which the Jacobian matrix is noninvertible ($\beta_3 = 0$). When this critical value is crossed, the two fixed points exchange their stability. For $c < 3$, the fixed point H_1 is stable and H_2 unstable, whereas for $c > 3$ these stability properties are inverted. Physically, this bifurcation gives rise to a traveling wave of hydraulic jump type. In the case of complex conjugated eigenvalues crossing, the generic situation is a Hopf bifurcation. There is no violation of the implicit function theorem since the Jacobian matrix remains invertible. At the bifurcation appears a limit cycle centered at the fixed point, this means that periodic solution may bifurcate from the uniform flow under suitable conditions. It is straightforward to show that the appearance of a Hopf bifurcation requires the following three conditions:

$$\beta_1\delta^{-1} > 0, \qquad \beta_2\delta^{-1} > 0, \qquad \beta_1\beta_2 = \delta\beta_3. \tag{54}$$

In order to illustrate the influence of all parameters on the possible bifurcations, we present results in the $(c, \cot\theta/R)$ plane for various R and W. First of all, it is to be noted that the equality in (54) is nothing but the marginal stability condition in the particular case of traveling waves. Moreover, the first two conditions are satisfied only in the linear instability regime ($R > R_c$). This allows to restrict ourselves to the values of $\cot\theta/R$ less than 6/5. Fig. 5 displays the effect of W on the Hopf bifurcation threshold ($\beta_1\beta_2 = \delta\beta_3$) represented by the curve (H). This curve converges naturally to the critical point ($\cot\theta/R = 6/5, c = 3$) and lies in a region ($R_1$) that is bounded by the curves $c = 3$ and $\beta_2 = 0$ and where the two inequalities in (54) are satisfied. It is seen that as W is decreased, the curve (H) tends towards the boundary (C) for which $\beta_2 = 0$. For relatively small W and beyond a some critical value, (H) is situated in both sides of (C). When W is further decreased the Hopf bifurcation threshold finally stands out of R_1 as $W \to 0$. This suggests that the Weber number must exceed a certain minimum value (W_m) for a Hopf bifurcation to occur. This minimum is obtained for each $\cot\theta/R$ by imposing that equations $\beta_1\beta_2 = \delta\beta_3$ and $\beta_2 = 0$ hold simultaneously. Since $\beta_3 \neq 0$ when $\beta_2 = 0$, it follows that $\delta = 0$. The elimination of c between these two conditions allows to express the minimum Weber number as a function of $\cot\theta/R$. Fig. 6 shows that there is discernible difference between the present model and that of Lee and Mei [27] who found that a more important W_m is required to destabilize the fixed point via Hopf bifurcation. Multiplying W_m by $R/3$, one obtains the minimum modified Weber number W'_m for the Hopf bifurcation to occur. Indeed, for small to moderate values of R, W'_m also is small and the occurrence of this unphysical frontier in the parameter space is not important since the whole long wave strategy is no longer valid. The presence of this minimum however could be significant in the limit of large R and therefore constitutes a defect of the model. This unrealistic phenomenon is related to the degeneracies of the system (48) coming from the possible cancellation of the denominator δ. It is revealed only by third order models incorporating inertia forces in the normal direction and could be cured by including higher order terms. In order to anticipate the effects of the various parameters on the appearance of complex attractors by a numerical procedure, the qualitative properties of the eigenvalues are shown by their location in the complex plane through Figs. 7. The distribution of the eigenvalues shows that complex dynamic may occur by crossing the Hopf bifurcation curve. In order to illustrate the role of W and R, typical values of these parameters are chosen to calculate the eigenvalues for various domains of the $\cot\theta/R$ versus c plane. The range of c is between $c = 1$ and another limit (of approximately 8.8) given in Fig. 4. When c lies above this upper limit, neither Hopf bifurcation nor heteroclinic orbits are possible whereas for $c < 1$, only the fixed points H_1 exists which does no longer undergo Hopf bifurcations. Fig. 7(a) depicts the qualitative properties of the eigenvalues for $W = 1$ and $R = 10$. It shows that for $c_h(\cot\theta)/R < c < 3$ where c_h indicates the critical value of c for the Hopf bifurcation to occur at some given $\cot\theta/R$, the fixed point H_1 is stable whereas the fixed point H_2 is unstable. Since no singularity intrudes between them, a heteroclinic orbit arising from H_2 and joining it to H_1, is therefore possible. By increasing c, the fixed point H_1 loses its stability when c crosses the critical value $c = 3$ and may undergo a transcritical bifurcation if c does not exceed the singular value of c which is of order 3.4 in the present case. When the Hopf line is crossed by decreasing c, a limit cycle bifurcates from the fixed point H_1, which in turn may undergo further complicated bifurcations if c is decreased again while remaining above

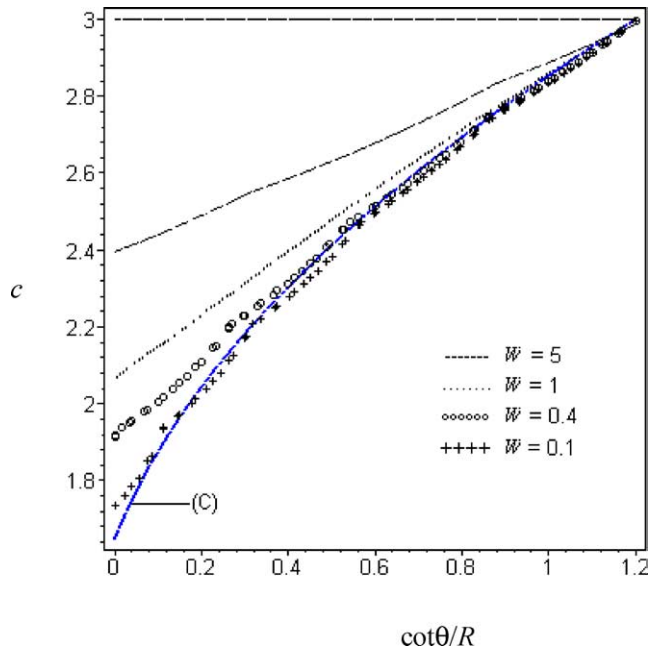

Fig. 5. Effects of the Weber number on the Hopf bifurcation threshold in the c versus $\cot\theta/R$ plane. For a Hopf bifurcation to occur, the value of c for a given $\cot\theta/R$ must be greater than that given by the curve (C) corresponding to $\beta_2 = 0$.

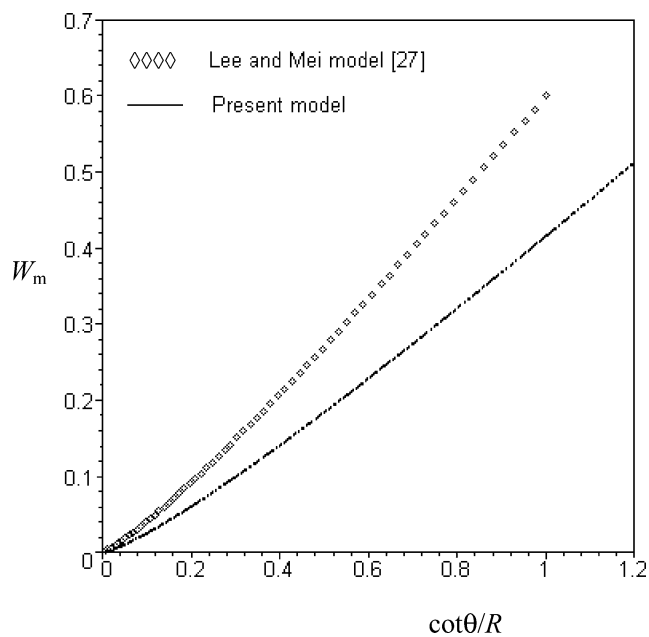

Fig. 6. Minimum Weber number for a Hopf bifurcation to occur from the Nusselt flow. The model does not predict the occurrence of a periodic flow if $W < W_m$.

the limit c_{1b} determined by the boundary (B). Besides the singular straightline (D) corresponding to the vanishing of $\delta(1)$ for a fixed W, the Hopf line (H) and the transcritical bifurcation threshold (T), we have also drawn:

(i) the curve (S), in the case of a saddle focus fixed point, along which the sum of the real eigenvalue and the real part of the complex ones vanishes; this curve referred as Shil'nikov boundary is described by the relation:

$$2\beta_1^3 + R^2\delta(1)\big[\beta_3\delta(1) + \beta_1\beta_2\big] = 0. \tag{55}$$

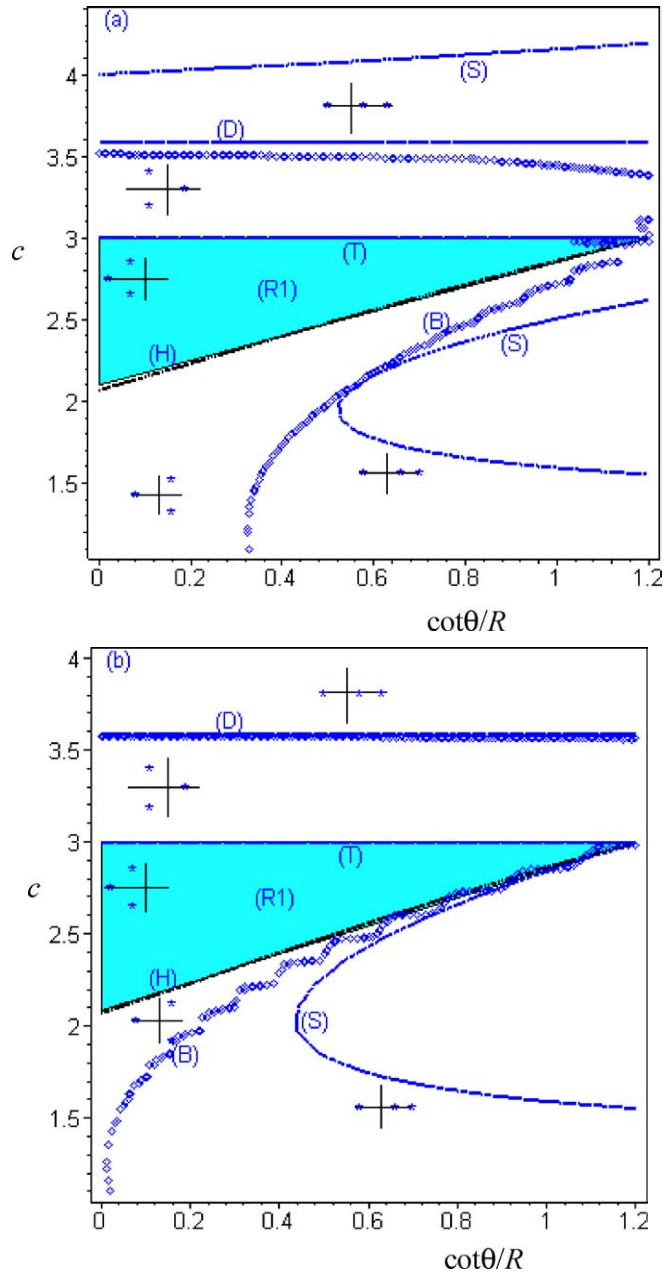

Fig. 7. Effect of W and R on the qualitative properties of the eigenvalues of the Jacobian matrix and location of the Hopf line (H), Shil'nikov line (S), line (B) separating saddle spirals from saddle nodes, straight lines (D) and (T) corresponding respectively to the singularity $\delta(1) = 0$ and to the transcritical bifurcation. (a) $W = 1$, $R = 10$; (b) $W = 1$, $R = 100$; (c) $W = 5$, $R = 10$; (d) $W = 5$, $R = 100$. The upstream fixed point is linearly stable in the region (R_1) between (T) and (H).

Crossing this curve may lead to homoclinic chaos according to the Shil'nikov theorem which stipulates that the existence of a homoclinic orbit generated by a saddle spiral fixed point implies the existence of nonperiodic trajectories if the magnitude of the real part of the complex eigenvalue is smaller than the magnitude of the real eigenvalue. Let us recall that a homoclinic orbit occurs when the trajectory that spirals out (or in) on the manifold spanned by the eigenvectors corresponding to the pair of complex eigenvalues eventually joins the trajectory coming into (or out of) the fixed point along a direction transverse to the spiral manifold.

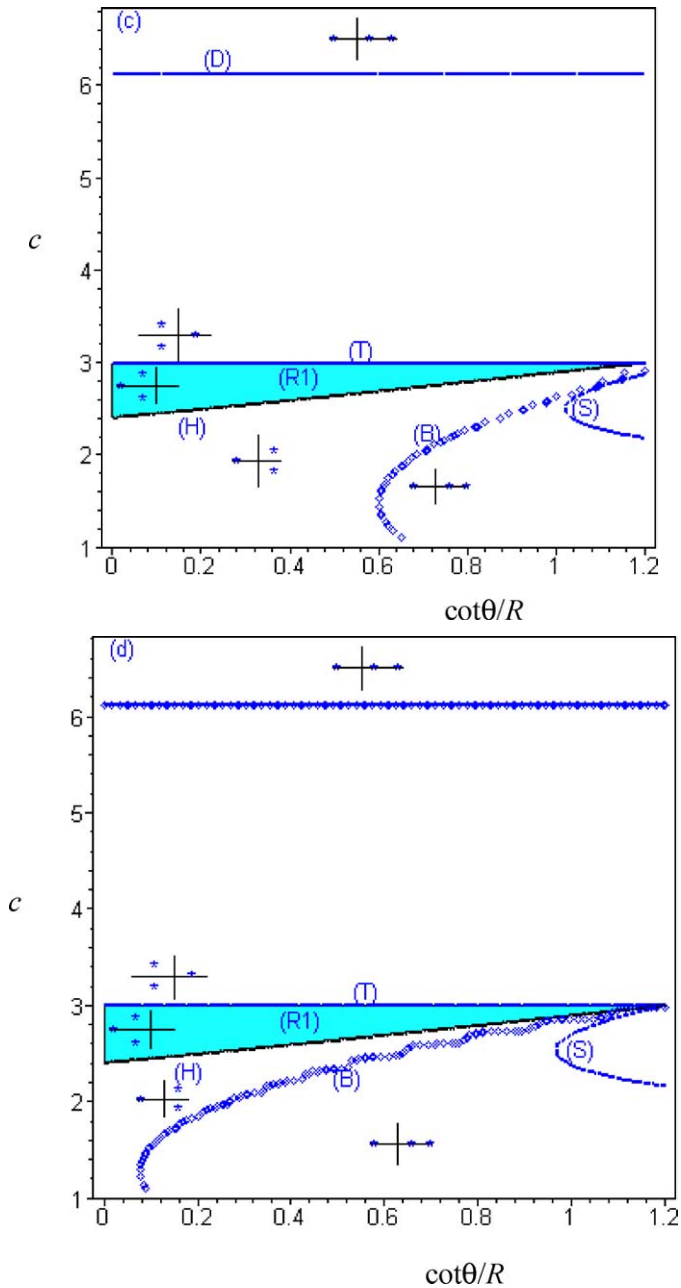

Fig. 7. Continued.

(ii) the boundary (B) separating saddle spirals from saddle nodes and along which two eigenvalues coalesce on the real axis. This property allows to represent it by the equation:

$$4R^2\left(\frac{\beta_1^2}{R^2} - 3\delta(1)\,\beta_2\right)\left(\beta_2^2 - 3\frac{\beta_1\beta_3}{R^2}\right) - (\beta_1\beta_2 - 9\,\delta(1)\beta_3)^2 = 0. \tag{56}$$

Crossing this curve may also lead, in some conditions, to Shil'nikov chaos.

We observe that Shil'nikov homoclinic chaos may occur in the whole region between the curves (H) and (B) since the Shil'nikov criteria is always satisfied here due to the curve (S) does not intersect the curve (B). Figs. 7(b)–(d) display how the Reynolds and the Weber numbers act upon the qualitative properties of the eigenvalues. The position of the boundary (B) is

seen to strongly depend on the Reynolds number for a given Weber number. The result is the shrinkage of the region where complex attractors are possible. Thence, it should be pointed out that chaotic motion may exist in the permanent wave form for only a small range of c, the size of which is a decreasing function of R at a given $\cot\theta/R$. It is seen that as W is increased, at fixed R, the boundary (H) qualitatively changes little whereas the change is drastic on the value of c_h and on the curve (B). We note again that for the present cases there is no singularity between the stable and unstable fixed points. This means that smooth heteroclinic orbit may therefore connect these fixed points when the transcritical value of c is crossed.

6.2. Numerical integration of the traveling wave equation

Here we shall discuss some results obtained by integrating (48) subject to appropriate initial conditions on **H**. These conditions were varied by superimposing an arbitrary small perturbation of magnitude of about 0.1% to the Nusselt solution. The integration is achieved by use of Maple 8 software library. Each run is pursed for sufficiently long time until the trajectories finally settle down on the attractor. We restrict our attention to the presentation of sample results, for $W = 1$ and $R = 10$. These are not exhaustive but provide a same qualitative picture of model behavior in certain regions of (W, R) space. As it is mentioned previously, the linear stability analysis also suggests to take the inclination θ so that $0 \leqslant \cot\theta/R \leqslant 6/5$. It was confirmed, through numerical experiments, that no nonlinear attractor exists when $\cot\theta/R > 6/5$. In order to illustrate how the behavior of solutions changes by continuously changing the wavespeed c, we first consider the transcritical bifurcation from H_1 to H_2 when the critical wavespeed $c = 3$ is crossed. Hence, a smooth connection may join the two fixed points provided that c remains below its singular value. In Fig. 8, we give the shape of the surface when H_1 corresponding to a heteroclinic orbit going from H_1 to H_2 for $\cot\theta/R = 0.2$ and $c = 3.1$. Similar results were obtained for other values of $\cot\theta/R$ and c. In accordance with the predictions of the linear analysis, there is no smooth heteroclinic orbit beyond the singular value of c. We now consider the more complex dynamics resulting from the first symmetry breaking via Hopf bifurcation. In order to illustrate the main features of the bifurcation scenarios beyond the Hopf thresholds we shall present attractors obtained for some selected values of c and $\cot\theta/R$. In the case of $\cot\theta/R = 0$, the fixed point first undergoes a Hopf bifurcation at $c_1 = 2.0701$, this generates a limit cycle whose period is of order $T = 7.6$. When c is decreased again, the limit cycle increases its amplitude and wavelength until a second critical value $c_2 = 1.9618$ is reached, where another limit cycle of period $2T$ takes place. Instead of a single maximum and single minimum the signal contains two maxima and two minima. Solutions remain $2T$ periodic as the phase velocity decreases until a further period doubling bifurcation occurs at approximately $c_3 = 1.9425$, the solution now being periodic with period $4T$ and the signal containing four maxima and four minima. It has been established by decreasing further the wave speed that a period doubling route to chaos is dictating the dynamics according to the Feigenbaum scenario.

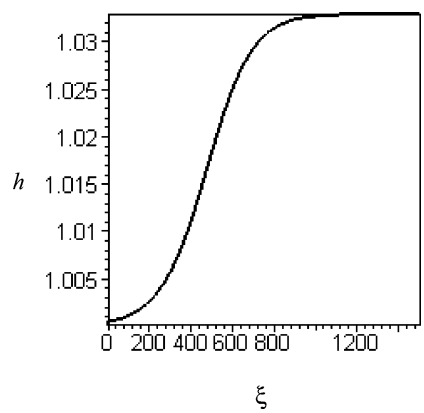

Fig. 8. Wave profile corresponding to heteroclinic orbit joining H_1 and H_2 and obtained for $W = 1$, $R = 10$, $\cot\theta/R = 0.2$ and $c = 3.1$. The prescribed initial conditions are $h(0) = 0.0001$, $h_\xi(0) = 0.001$ and $h_{\xi\xi}(0) = 0.001$.

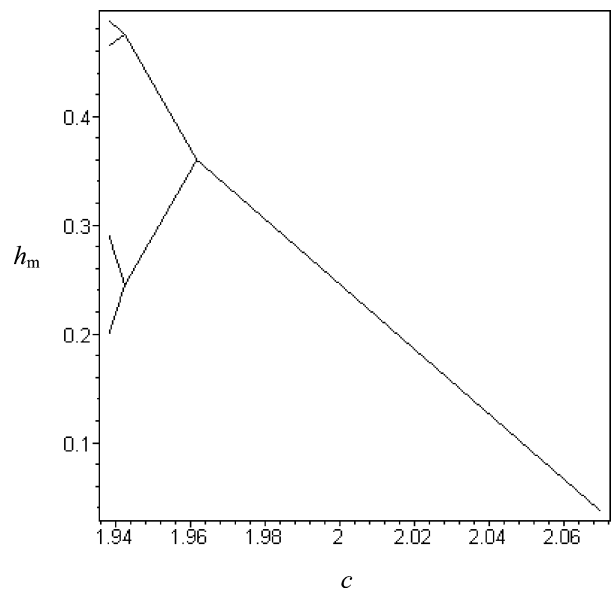

Fig. 9. Global bifurcation diagram showing the local maxima h_m of the wave profile plotted against the wave celerity in the case of vertical plane for $R = 10$, $W = 1$. This illustrates the period doubling bifurcations leading to chaos.

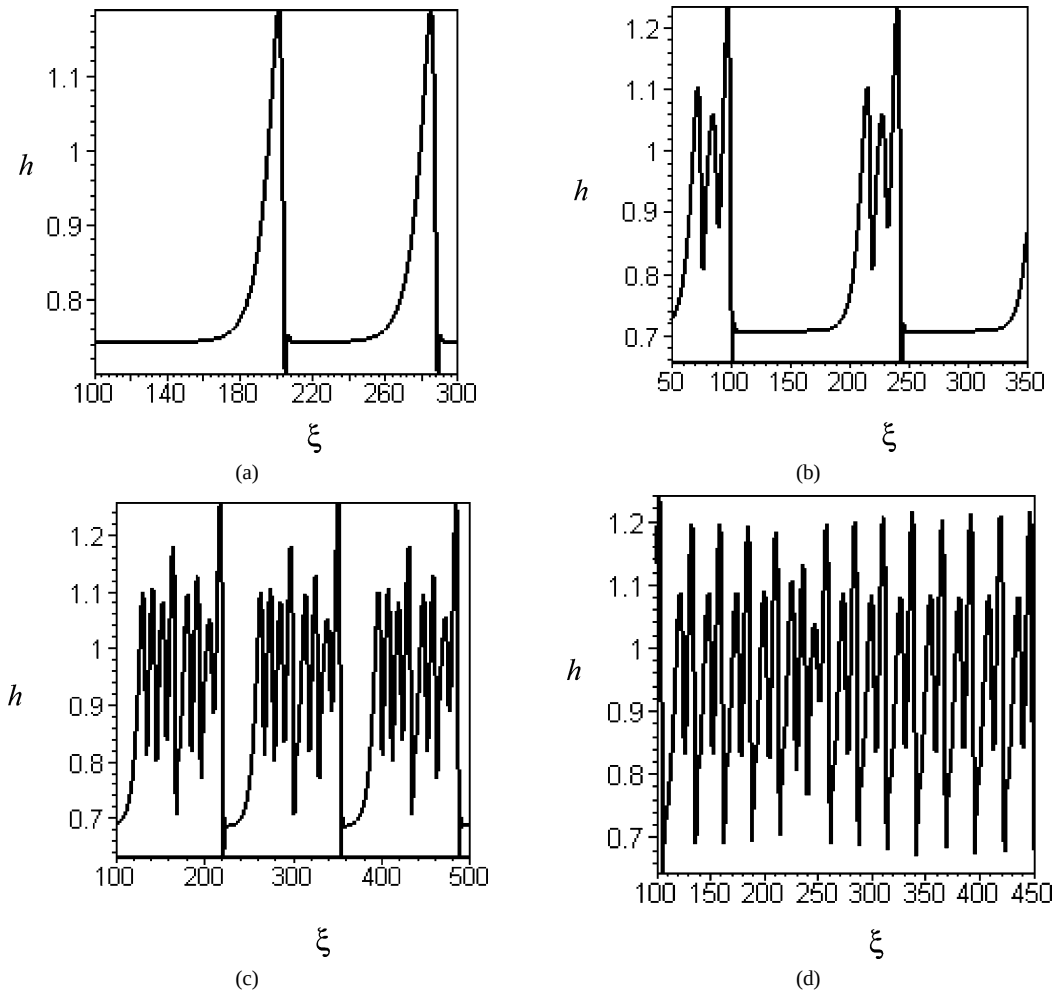

Fig. 10. More and more complex solitary waves leading to homoclinic chaos are obtained by decreasing $\cot\theta/R$ and c (a) $\cot\theta/R = 0.4$, $c = 2.294971796$, (b) $\cot\theta/R = 0.30$, $c = 2.20949805451$, (c) $\cot\theta/R = 0.25$, $c = 2.1577077995$, (d) $\cot\theta/R = 0.20$, $c = 2.110098$. The prescribed initial conditions are: $h(0) = 0.001$, $h_\xi(0) = 0.01$, $h_{\xi\xi}(0) = 0.01$ for the cases (a), (c), (d) and $h(0) = 0.001$, $h_\xi(0) = 0.001$, $h_{\xi\xi}(0) = 0.01$ for the case (b).

Table 1
Successive bifurcation points compared with those obtained from the models presented in [26] and [27]

c	c_1	c_2	c_3	c_0	c_∞
Present model	2.2060	2.1806	2.1751	2.1745	2.120805078
Nguyen and Balakotaiah [26]	2.4400	2.3044	–	2.2496	2.219249700
Lee and Mei [27]	2.2824	2.2581	2.2545	2.2536	2.198575538

These results are summarized in Fig. 9 which displays the bifurcation diagram representing the maximal wave amplitude as a function of the wave speed. The periodic character of the wave is preserved by decreasing c until the critical value $c_0 = 1.9371$ is reached. Decreasing the celerity further causes the waves to lose their regularity and degenerate into chaotic attractor until another critical value $c_\infty = 1.8639$ is reached. Beyond this limiting value, the solution become unbounded. It can be seen from the computed values of successive window lengths that our results are consistent with the Feigenbaum universal theory. For testing the model, we compare in Table 1 the successive bifurcation points with those given in [26] and [27] for the same set of parameter values, namely $R = 3.8$ and $Ka = 22$. Further calculations were carried out for various $\cot\theta/R$. First of all, we note that beyond the first symmetry breaking, the amplitude and the wavelength of the resulting limit cycle grow with $\cot\theta/R$. We found again that reducing c for various $\cot\theta/R$ leads to other bifurcation scenarios. Figs. 10 show attractors constituted by a

series of solitary waves forming a train of periodic waves with very long periods, obtained for some values of $\cot\theta/R$ and c. These waves are characterized by one or more prominent peaks, a gentle slope at the upstream side and a steep wave front due to gravity and preceded by capillary ripples. These peculiar forms suggest near homoclinic bifurcations. The orbits slowly rise from H_2, wind one or several times around $H_1$and then return to H_2. By decreasing $\cot\theta/R$, the dynamics becomes more and more complex and homoclinic chaos is expected by further decreasing of $\cot\theta/R$.

7. Concluding remarks

The main contribution of this paper consists in the incorporation of third order terms which should be taken into account, for consistency, in the range of small to moderate Weber numbers. Neglecting these terms, particularly in the high Reynolds number range amounts to inconsistently omitting some second order terms in the dynamics of the film flow. The efficiency and accuracy of the model are illustrated by comparing the linear stability results with those given by some recent models and the OS equation. The ability of the model to follow quite closely the numerical results given by the OS equation is due to a suitable choice of the parameter α introduced to describe the second order departure of the velocity profile. Improvements appear significantly in the limit of small Weber numbers corresponding to inertia dominated regimes. The nonlinear aspects of the film flow are then examined by using a simplified version of the model that however retains its main features and by considering asymptotic states characterized by waves of permanent form. In the relatively limited subspace of parameters we have explored, the solutions exhibit the same qualitative behaviors as those given by other authors. Quantitatively, some differences are found and deserve to be reported. For example it is found that the predicted minimum Weber number for a Hopf bifurcation to occur is approximately 30% less, and therefore closer to reality, than that given by Lee and Mei [27]. The occurrence of this threshold has no importance for small to moderate Reynolds numbers since the long wave assumption is no longer valid but rather constitutes a shortcoming of the model in the limit of large Reynolds numbers; this may be cured for instance by the inclusion of higher order terms.

Appendix

$$
\begin{aligned}
Q_1(q,h,s_1,s_2) &= \frac{1}{R}\left(\frac{5}{2}\frac{q}{h^2}-\frac{5}{2}h+\frac{5}{2}hh_x\cot\theta+\frac{9}{2}\frac{h_xq_x}{h}-4\frac{h_x^2q}{h^2}+6\frac{h_{xx}q}{h}-\frac{9}{2}q_{xx}\right)+\frac{18}{7}\frac{qs_2h_x}{h^2}+4\frac{qs_1h_x}{h^2}\\
&\quad-\frac{27}{14}\frac{qs_{2x}}{h}-3\frac{qs_{1x}}{h}+\frac{17}{7}\frac{qq_x}{h}-\frac{9}{7}\frac{q^2h_x}{h^2}-\frac{17}{7}\frac{s_2q_x}{h}-\frac{13}{3}\frac{s_1q_x}{h}-\frac{5}{6}Whh_{xxx},\\
\widetilde{Q}_1(q,h,s_1,s_2) &= \frac{115}{672}\frac{q^2h_x^3}{h^2}+\frac{95841}{2002}\frac{s_2s_{2x}}{h}-\frac{23337}{1001}\frac{s_2^2h_x}{h^2}-\frac{1251}{143}\frac{s_2s_{1x}}{h}-\frac{261}{143}\frac{s_1s_{2x}}{h}+\frac{238}{11}\frac{s_1s_{1x}}{h}\\
&\quad-\frac{112}{11}\frac{s_1^2h_x}{h^2}-\frac{11}{56}hq_{xt}h_x-\frac{187}{1344}qq_{xx}h_x+\frac{4633}{2688}qq_xh_{xx}-\frac{601}{1008}hqq_{xxx}-\frac{683}{1008}hq_xq_{xx}\\
&\quad+\frac{107}{336}q_thh_{xx}+\frac{29}{56}q_th_x^2+\frac{509}{672}q_x^2h_x-\frac{253}{672}\frac{qq_xh_x^2}{h}+\frac{828}{143}\frac{s_1s_2h_x}{h^2}-\frac{11}{56}h^2q_{xxt}\\
&\quad+\frac{1205}{2688}q^2h_{xxx}-\frac{555}{896}\frac{q^2h_{xx}h_x}{h}+\frac{1}{R}\left(\frac{51}{8}s_{1xx}-\frac{71}{32}s_{2xx}-\frac{181}{8}\frac{s_{1x}h_x}{h}+\frac{137}{8}\frac{s_1h_x^2}{h^2}\right.\\
&\quad\left.-\frac{391}{16}\frac{s_1h_{xx}}{h}+\frac{1577}{64}\frac{s_{2x}h_x}{h}-\frac{1379}{64}\frac{s_2h_x^2}{h^2}+\frac{3197}{128}\frac{s_2h_{xx}}{h}\right),\\
S_1(q,h,s_1,s_2) &= \frac{1}{R}\left(\frac{3}{10}\frac{q}{h^2}-\frac{3}{10}h+\frac{3}{10}hh_x\cot\theta+\frac{126}{5}\frac{s_1}{h^2}+\frac{126}{5}\frac{s_2}{h^2}+\frac{9}{40}q_{xx}+\frac{69}{40}\frac{h_xq_x}{h}\right.\\
&\quad\left.-\frac{93}{40}\frac{h_x^2q}{h^2}-\frac{21}{80}\frac{h_{xx}q}{h}\right)+\frac{103}{55}\frac{s_1q_x}{h}-\frac{10557}{10010}\frac{qs_{2x}}{h}+\frac{5022}{5005}\frac{qs_2h_x}{h^2}\\
&\quad-\frac{108}{55}\frac{qs_1h_x}{h^2}-\frac{9657}{5005}\frac{s_2q_x}{h}-\frac{1}{35}\frac{qq_x}{h}+\frac{3}{35}\frac{q^2h_x}{h^2}+\frac{39}{55}\frac{qs_{1x}}{h}-\frac{1}{10}Whh_{xxx},\\
\widetilde{S}_1(q,h,s_1,s_2) &= \frac{2943}{715}\frac{s_1s_{2x}}{h}+\frac{3033369}{170170}\frac{s_2s_{2x}}{h}-\frac{187}{2240}q_th_x^2-\frac{97}{1680}h^2q_{xxt}-\frac{45009}{6545}\frac{s_2^2h_x}{h^2}-\frac{168}{715}\frac{s_1^2h_x}{h^2}
\end{aligned}
$$

$$
\begin{aligned}
&+\frac{7893}{715}\frac{s_2 s_{1x}}{h}+\frac{798}{715}\frac{s_1 s_{1x}}{h}+\frac{209}{2240}q_{xt}hh_x+\frac{433}{4480}q_t hh_{xx}-\frac{3636}{715}\frac{s_1 s_2 h_x}{h^2}\\
&+\frac{1}{R}\Big(-\frac{59}{40}s_{1xx}-\frac{81}{160}s_{2xx}-\frac{19}{40}\frac{s_{1x}h_x}{h}-\frac{903}{80}\frac{s_{2x}h_x}{h}+\frac{393}{40}\frac{s_1 h_x^2}{h^2}-\frac{33}{10}\frac{s_2 h_x^2}{h^2}\\
&+\frac{37}{10}\frac{s_1 h_{xx}}{h}-\frac{3021}{320}\frac{s_2 h_{xx}}{h}\Big)+\Big(-\frac{817203}{1601600}+\frac{31969}{9815520}\alpha\Big)\frac{q^2 h_x h_{xx}}{h}\\
&+\Big(\frac{394347}{1601600}-\frac{4567}{981552}\alpha\Big)q_x^2 h_x+\Big(\frac{416167}{3203200}+\frac{4567}{4907760}\alpha\Big)q^2 h_{xxx}\\
&+\Big(\frac{824049}{1601600}+\frac{4567}{3271840}\alpha\Big)qq_x h_{xx}+\Big(-\frac{25791}{36400}+\frac{4567}{613470}\alpha\Big)\frac{qq_x h_x^2}{h}\\
&+\Big(\frac{336101}{800800}-\frac{31969}{14723280}\alpha\Big)qq_{xx}h_x+\Big(\frac{613057}{1601600}-\frac{4567}{1635920}\alpha\Big)\frac{q^2 h_x^3}{h^2}\\
&-\Big(\frac{168139}{960960}+\frac{4567}{7361640}\alpha\Big)hqq_{xxx}-\Big(\frac{20705}{96096}+\frac{4567}{2944656}\alpha\Big)hq_x q_{xx},
\end{aligned}
$$

$$
\begin{aligned}
S_2(q,h,s_1,s_2)=&\frac{1}{R}\Big(\frac{13}{140}\frac{q}{h^2}-\frac{13}{140}h+\frac{39}{5}\frac{s_1}{h^2}+\frac{11817}{140}\frac{s_2}{h^2}+\frac{13}{140}hh_x\cot\theta-\frac{559}{2240}q_{xx}-\frac{2613}{4480}\frac{h_x q_x}{h}\\
&+\frac{3211}{4480}\frac{h_x^2 q}{h^2}+\frac{2847}{8960}\frac{h_{xx}q}{h}\Big)+\frac{19}{11}\frac{s_2 q_x}{h}+\frac{288}{385}\frac{qs_{2x}}{h}+\frac{2}{33}\frac{s_1 q_x}{h}+\frac{4}{11}\frac{qs_1 h_x}{h^2}\\
&-\frac{6}{55}\frac{qs_{1x}}{h}-\frac{18}{11}\frac{qs_2 h_x}{h^2}-\frac{13}{420}Whh_{xxx},
\end{aligned}
$$

$$
\begin{aligned}
\widetilde{S}_2(q,h,s_1,s_2)=&-\frac{18}{935}\frac{s_1 s_{2x}}{h}+\frac{37251}{14630}\frac{s_2 s_{2x}}{h}-\frac{288}{209}\frac{s_2^2 h_x}{h^2}+\frac{1467}{935}\frac{s_2 s_{1x}}{h}-\frac{14}{55}\frac{s_1 s_{1x}}{h}\\
&-\frac{14}{11}\frac{s_1^2 h_x}{h^2}-\frac{432}{187}\frac{s_1 s_2 h_x}{h^2}+\frac{1}{R}\Big(\frac{13}{80}s_{1xx}-\frac{4831}{2240}s_{2xx}+\frac{2379}{640}\frac{s_{1x}h_x}{h}+\frac{13393}{4480}\frac{s_{2x}h_x}{h}\\
&-\frac{5473}{640}\frac{s_1 h_x^2}{h^2}+\frac{158953}{8960}\frac{s_2 h_x^2}{h^2}-\frac{351}{1280}\frac{s_1 h_{xx}}{h}+\frac{63641}{17920}\frac{s_2 h_{xx}}{h}\Big)\\
&-\Big(\frac{4331}{177408}+\frac{54051}{239599360}\alpha\Big)hq_x q_{xx}+\Big(\frac{70957}{1478400}+\frac{906539}{102685440}\alpha\Big)h_x q_x^2\\
&+\Big(\frac{97133}{11827200}-\frac{48498889}{23001538560}\alpha\Big)q^2 h_{xxx}+\Big(\frac{289}{17920}-\frac{4567}{1921920}\alpha\Big)h_x^2 q_t\\
&+\Big(-\frac{25}{5376}+\frac{4567}{5765760}\alpha\Big)h^2 q_{xxt}+\Big(\frac{566047}{11827200}-\frac{53033479}{23001538560}\alpha\Big)qq_x h_{xx}\\
&-\Big(\frac{9923}{268800}+\frac{26801219}{1437596160}\alpha\Big)\frac{qq_x h_x^2}{h}+\Big(-\frac{1447}{5913600}+\frac{2696803}{289935360}\alpha\Big)qq_{xx}h_x\\
&+\Big(\frac{2687}{1478400}+\frac{509217}{68456960}\alpha\Big)\frac{q^2 h_x^3}{h^2}+\Big(-\frac{22909}{1774080}+\frac{89492281}{34502307840}\alpha\Big)hqq_{xxx}\\
&+\Big(\frac{893}{107520}-\frac{4567}{3843840}\alpha\Big)hh_{xx}q_t+\Big(-\frac{107}{17920}+\frac{4567}{1921920}\alpha\Big)hh_x q_{xt}\\
&-\Big(\frac{50073}{3942400}+\frac{9232117}{1353031680}\alpha\Big)\frac{q^2 h_{xx}h_x}{h},
\end{aligned}
$$

$$
\begin{aligned}
Q_2(q,h,s_1,s_2)=&\frac{1}{R}\Big(\frac{81}{28}\frac{q}{h^2}-\frac{81}{28}h+\frac{81}{28}hh_x\cot\theta+\frac{10851}{1792}\frac{h_{xx}q}{h}-\frac{2027}{448}q_{xx}+\frac{3069}{28}\frac{s_2}{h^2}+33\frac{s_1}{h^2}\\
&+\frac{5055}{896}\frac{h_x q_x}{h}-\frac{5025}{896}\frac{h_x^2 q}{h^2}\Big)+\frac{126}{65}\frac{qs_2 h_x}{h^2}+\frac{12}{5}\frac{qs_1 h_x}{h^2}-\frac{1017}{455}\frac{qs_{2x}}{h}-\frac{12}{5}\frac{qs_{1x}}{h}\\
&+\frac{12}{5}\frac{qq_x}{h}-\frac{6}{5}\frac{q^2 h_x}{h^2}-\frac{171}{65}\frac{s_2 q_x}{h}-\frac{12}{5}\frac{s_1 q_x}{h}-\frac{27}{28}Whh_{xxx},
\end{aligned}
$$

$$
\begin{aligned}
\widetilde{Q}_2(q,h,s_1,s_2) = {} & \frac{2124}{935}\frac{s_1 s_{2x}}{h} + \frac{220649697}{3233230}\frac{s_2 s_{2x}}{h} - \frac{7290594}{230945}\frac{s_2^2 h_x}{h^2} + \frac{3609}{935}\frac{s_2 s_{1x}}{h} + \frac{16086}{715}\frac{s_1 s_{1x}}{h} \\
& - \frac{8358}{715}\frac{s_1^2 h_x}{h^2} - \frac{19512}{12155}\frac{s_1 s_2 h_x}{h^2} + \frac{1}{R}\left(\frac{81}{16}s_{1xx} - \frac{2187}{448}s_{2xx} - \frac{2481}{128}\frac{s_{1x}h_x}{h} + \frac{14643}{896}\frac{s_{2x}h_x}{h}\right. \\
& \left. + \frac{2355}{128}\frac{s_1 h_x^2}{h^2} - \frac{12735}{1792}\frac{s_2 h_x^2}{h^2} - \frac{5379}{256}\frac{s_1 h_{xx}}{h} + \frac{68409}{3584}\frac{s_2 h_{xx}}{h}\right) \\
& - \left(\frac{21373}{23296} + \frac{4527437}{2548465920}\alpha\right) h q_x q_{xx} + \left(\frac{122497}{116480} + \frac{506717}{121355520}\alpha\right) h_x q_x^2 \\
& + \left(\frac{546453}{931840} - \frac{10673557}{9061212160}\alpha\right) q^2 h_{xxx} + \left(\frac{8073}{17920} - \frac{4567}{1921920}\alpha\right) h_x^2 q_t \\
& + \left(-\frac{2319}{8960} + \frac{4567}{5765760}\alpha\right) h^2 q_{xxt} + \left(\frac{2130151}{931840} - \frac{24731633}{27183636480}\alpha\right) q q_x h_{xx} \\
& - \left(\frac{261369}{232960} + \frac{6342023}{566325760}\alpha\right) \frac{q q_x h_x^2}{h} + \left(\frac{130609}{465920} + \frac{162875}{22843392}\alpha\right) q q_{xx} h_x \\
& + \left(\frac{64731}{116480} + \frac{375943}{80903680}\alpha\right) \frac{q^2 h_x^3}{h^2} + \left(-\frac{182667}{232960} + \frac{8940823}{4530606080}\alpha\right) h q q_{xxx} \\
& + \left(\frac{3035}{7168} - \frac{4567}{3843840}\alpha\right) h h_{xx} q_t + \left(-\frac{391}{3584} + \frac{4567}{1921920}\alpha\right) h h_x q_{xt} \\
& - \left(\frac{1064499}{931840} + \frac{1900881}{533012480}\alpha\right) \frac{q^2 h_{xx} h_x}{h}.
\end{aligned}
$$

Acknowledgements

The authors would like to warmly thank the referees for their attention to the manuscript and their helpful comments and suggestions.

References

[1] I.L. Kliakhandler, G.I. Sivashinsky, Viscous damping and instabilities in stratified liquid film flowing down a slightly inclined plane, Phys. Fluids 9 (1) (1996) 23–30.
[2] W. Nusselt, Die oberflachenkondensation des Wasserdampfes, Z. Ver. Dtsch. Ing. 60 (1916) 541–552.
[3] H.C. Chang, Wave evolution on a falling film, Ann. Rev. Fluid Mech. 26 (1994) 103–136.
[4] A. Oron, O. Gottlieb, Nonlinear dynamics of temporally excited falling liquid films, Phys. Fluids 14 (8) (2002) 2622–2636.
[5] J. Liu, J.D. Paul, J.P. Gollub, Measurements of the primary instability of film flow, J. Fluid Mech. 250 (1993) 69–101.
[6] J. Liu, J.P. Gollub, Solitary wave dynamics of film flows, Phys. Fluids 6 (1994) 1702–1711.
[7] J. Liu, J.B. Schneider, J.P. Gollub, Three dimensional instabilities of film flows, Phys. Fluids 7 (1995) 55–67.
[8] P.L. Kapitza, S.P. Kapitza, Wave flow of thin layers of viscous fluid, Zh. Ekper. Teor. Fiz. 19 (1949) 105.
[9] N. Brauner, D.M. Maron, Characteristics of inclined thin film. Waviness and the associated mass transfer, Int. J. Heat Mass Transfer 25 (1982) 99–110.
[10] T.B. Benjamin, Wave formation in laminar flow down an inclined plane, J. Fluid Mech. 2 (1957) 554–574.
[11] C.S. Yih, stability of liquid flow down an inclined plane, Phys. Fluids 6 (1963) 321–330.
[12] A.P. Hooper, W.G.C. Boyd, Shear flow instability at the interface between two viscous fluids, J. Fluid Mech. 128 (1983) 507–528.
[13] R.E. Kelly, D.A. Goussis, S.P. Lin, F.K. Hsu, The mechanism of surface wave instability in film flow down an inclined plane, Phys. Fluids 1 (1989) 819–828.
[14] L. Brevdo, P. Laure, F. Dias, T.J. Bridges, Linear pulse structure and signalling in a film flow on an inclined plane, J. Fluid Mech. 396 (1999) 37–71.
[15] P. Bach, J. Villadsen, Simulation of the vertical flow of a thin, wavy film using a finite-element method, Int. J. Heat Mass Transfer 27 (1984) 815–827.
[16] H.S. Kheshgi, L.E. Scriven, Disturbed film flow on a vertical plate, Phys. Fluids 30 (1987) 990–997.
[17] W. Choi, R. Camassa, Fully nonlinear internal waves in a two-fluid system, J. Fluid Mech. 396 (1999) 1–36.
[18] D.J. Benney, Long waves on liquid films, J. Math. Phys. 45 (1966) 150–155.

[19] A. Pumir, P. Manneville, Y. Pomeau, On solitary waves running down an inclined plane, J. Fluid Mech. 135 (1983) 27–50.
[20] P. Rosenau, A. Oron, J.M. Hyman, Bounded and unbounded patterns of the Benney equation, Phys. Fluids A 4 (1992) 1102–1104.
[21] G.I. Sivashinsky, D.M. Michelson, On irregular wavy flow of a liquid film down a vertical plane, Prog. Theor. Phys. 63 (1980) 2112–2114.
[22] J. Topper, T. Kawahara, Approximate equations for long nonlinear waves on a viscous fluid, J. Phys. Soc. Japan 44 (1974) 663–666.
[23] T. Ooshida, Surface equation of falling film flows with moderate Reynolds number and large but finite Weber number, Phys. Fluids 11 (1999) 3247–3269.
[24] M.K.R. Panga, V. Balakotaiah, Low dimensional models for vertically falling viscous films, Phys. Rev. Lett. 90 (15) (2003) 1–4.
[25] V.Y. Shkadov, Wave conditions in the flow of thin layer of a viscous liquid under the action of gravity, Izv. Akad. Nauk SSSR, Mekh. Zhidk. Gaza 1 (1967) 43–51.
[26] L.T. Nguyen, V. Balakotaiah, Modeling and experimental studies of wave evolution on free falling viscous films, Phys. Fluids 12 (2000) 2236–2256.
[27] J.J. Lee, C.C. Mei, Stationary waves on an inclined sheet of viscous fluid at high Reynolds and moderate Weber numbers, J. Fluid Mech. 307 (1996) 191–229.
[28] L.Q. Yu, F.K. Wadsen, A.E. Duckler, V. Balakotaiah, Nonlinear evolution of waves on falling films at high Reynolds number, Phys. Fluids 7 (1995) 1886–1902.
[29] I.L. Kliakhandler, Inverse cascade in film flows, J. Fluid Mech. 423 (2000) 205–225.
[30] C. Ruyer-Quil, P. Manneville, Modeling film flows down an inclined planes, Eur. Phys. J. B 6 (1998) 277–292.
[31] C. Ruyer-Quil, P. Manneville, Improved modeling of flows down inclined planes, Eur. Phys. J. B 15 (2000) 357–369.
[32] C. Ruyer-Quil, P. Manneville, Further accuracy and convergence results on the modeling of flows down inclined planes by weighted residual approximations, Phys. Fluids 14 (2002) 170–183.